Genome-wide transcriptional responses of iron-starved *Chlamydia trachomatis* reveal prioritization of metabolic precursor synthesis over protein translation

Amanda J. Brinkworth[1], Mark R. Wildung[1,2], Rey A. Carabeo[1#]

1. School of Molecular Biosciences, College of Veterinary Medicine, Washington State University.

2. Laboratory of Biotechnology and Bioanalysis, College of Veterinary Medicine, Washington State University.

#. Corresponding Author

Running title: Global response of *C. trachomatis* to iron-starvation

Abstract word count: 250

Importance word count: 147

Text word count (Introduction, Results, Discussion): 5139

Text word count (Introduction, Results, Discussion, Materials and Methods, Acknowledgements): 6058

ABSTRACT (exactly 250 words)

Iron is essential for growth and development of *Chlamydia*. Its long-term starvation in cultured mammalian cells leads to production of aberrant non-infectious chlamydial forms, also known as persistence. Immediate transcriptional responses to iron limitation have not been characterized, leaving a knowledge gap of how *Chlamydia* regulates its response to changes in iron availability. We used the fast-chelating agent 2,2'-Bipyridyl (BPDL) to homogeneously starve *Chlamydia trachomatis* serovar L2 of iron, starting at 6 or 12h post-infection. Immediate transcriptional responses were monitored after only 3 or 6h of BPDL-treatment, well before formation of aberrant *Chlamydia.* The first genome-wide transcriptional response of *C. trachomatis* to iron-starvation was subsequently determined utilizing RNA-sequencing. Only 7% and 8% of the genome was differentially expressed in response to iron-starvation at early and mid-stages of development, respectively. Biological pathway analysis revealed an overarching theme. Synthesis of macromolecular precursors (deoxynucleotides, amino acids, charged tRNAs, and acetyl-coA) was up-regulated, while energy-expensive processes (ABC transport and translation) were down-regulated. A large fraction of differentially down-regulated genes are involved in translation, including ribosome assembly, initiation and termination factors, which could be analogous to the translation down-regulation triggered by stress in other prokaryotes during stringent responses. Additionally, transcriptional up-regulation of DNA repair, oxidative stress, and tryptophan salvage genes reveals a possible coordination of responses to multiple antimicrobial and immunological insults. These responses of replicative-phase *Chlamydia* to iron-starvation indicate a prioritization of survival over replication, enabling the pathogen to

44 “stock the pantry” with ingredients needed for rapid growth once optimal iron levels are
45 restored.
46
47

48 IMPORTANCE (max 150 words, currently at 147)

49 By utilizing an experimental approach that monitors the immediate global response of
50 *Chlamydia trachomatis* to iron-starvation, clues to long-standing questions in *Chlamydia*
51 biology are revealed, including how *Chlamydia* adapts to this stress. We determined
52 that this pathogen initiates a transcriptional program that prioritizes replenishment of
53 nutrient stores over replication, possibly in preparation for rapid growth once optimal
54 iron levels are restored. Transcription of genes for biosynthesis of metabolic precursors
55 was generally up-regulated, while those involved in multiple steps of translation were
56 down-regulated. We also observed an increase in transcription of genes involved in
57 DNA repair and neutralizing oxidative stress, indicating that *Chlamydia* employs an "all-
58 or-nothing" strategy. Its small genome limits its ability to tailor a specific response to a
59 particular stress. Therefore, the "all-or-nothing" strategy may be the most efficient way
60 of surviving within the host, where the pathogen likely encounters multiple simultaneous
61 immunological and nutritional insults.
62

63 INTRODUCTION

64 The sexually transmitted bacterium *Chlamydia trachomatis* infects the mucosal
65 epithelium of the endocervix, urethra, and anogenital tract. These infections usually
66 resolve spontaneously, and most are asymptomatic and thus underreported. Over 1.5
67 million cases of *C. trachomatis* genital infections were reported in the US in 2015 alone
68 (1). As many as 17% of females infected with *C. trachomatis* develop long-term
69 infections in the genital tract, which can result in serious complications such as pelvic
70 inflammatory disease (PID), fallopian-tube scarring, and ectopic pregnancy, all of which
71 are major risk factors for tubal factor infertility (TFI) (2). In some patients, infection
72 persists even after antibiotic treatment (3, 4). The ability of *C. trachomatis* to survive
73 long-term in some individuals despite host immunity and antibiotic treatment is not well
74 understood, and may be associated with *Chlamydia*'s ability to become persistent (5).
75 While aberrant chlamydial forms have been identified in cervical samples, the clinical
76 relevance of this phenomenon is not well understood (5, 6).

77 Chlamydiae are obligate intracellular Gram-negative bacteria that undergo a
78 biphasic developmental cycle that includes both non-replicative and replicative forms
79 (7). Infection begins when the small, metabolically quiescent chlamydial elementary
80 body (EB) binds to mucosal epithelial cells and translocates virulence factors that
81 induce its endocytic uptake. Within 2 hours of entry, the EB will differentiate into its
82 replicative form, the reticulate body (RB). Continued secretion of effectors leads to
83 modification of the endocytic vesicle such that it avoids fusion with the lysosome and
84 enables capture of nutrient-rich vesicles. This unique intracellular niche, called the
85 inclusion, continues to expand as RBs replicate. In response to unknown signals around

24h post-infection, RBs will then differentiate into infectious EBs, followed by EB release 36-72 hours post-infection (7). Under exposure to certain stress conditions in cell culture (e.g. penicillin, interferon-gamma (IFN-g), iron-depletion or tryptophan-depletion) RBs will not differentiate into EBs, but instead enter into a state of persistence, characterized by aberrant, enlarged morphology (8–12). Persistent *Chlamydia* are resistant to both antibiotics and host immunity mechanisms, and can recover from this state upon removal of stress or addition of missing nutrients (13–16).

Chlamydiae have undergone reductive evolution as they have adapted to intracellular growth in mammalian cells, discarding metabolic genes responsible for synthesizing factors that could be acquired from the host (17). The core genome of *C. trachomatis* serovar L2 encodes only 889 open-reading frames, making *Chlamydia* dependent on its host for lipids, nucleotides, amino acids, and metal cofactors (17). Exposure of *Chlamydia*-infected cells to immune mediators, such as interferon-g, reduces the availability of these factors and results in reduced RB division and differentiation (11, 13). IFN-g induces intracellular depletion of tryptophan by increasing levels of indolamine 2,3-dioxygenase, which is responsible for catabolizing tryptophan into kynurenines, which cannot be utilized in tryptophan metabolism (18).

Induction of inflammatory cytokines such as interferon-g and IL-6 in response to chlamydial infection likely causes sequestration of free iron by the mononuclear phagocytic system, which includes both cellular and systemic regulatory pathways (19–26). Readers are referred to two comprehensive reviews of the coordinated regulation of iron homeostasis by systemic and cellular mechanisms (25, 27). In the context of

Chlamydia infection of the genital epithelium, iron availability in infected cells is likely limited by down-regulation of transferrin receptor and upregulation of the iron-storage factor, ferritin (28). Iron-levels in the female genital tract can also fluctuate throughout the menstrual cycle, in part due to hormone-induced expression of lactoferrin (29, 30). Iron is essential for growth and development of *Chlamydia*, and its acquisition and accumulation must be carefully regulated. In mammals, the readily usable ferrous iron (Fe^{2+}) is tied up in molecular complexes, limiting their interaction with hydrogen peroxide to form damaging hydroxyl radicals through the Fenton reaction (31). Eukaryotic stores of ferric iron (Fe^{3+}) are strictly regulated to restrict access by pathogenic bacteria (32). Extracellular bacteria such as *Pseudomonas* and *Yersinia* utilize multiple redundant iron-binding molecules called siderophores that compete with mammalian transferrin for ferrous iron (33, 34). Intracelllular bacteria, such as *Mycobacterium*, *Francisella* and *Chlamydia,* can obtain iron by subverting host vesicles that contain holo-transferrin bound to transferrin receptor (35–38). Using a combination of endocytic markers and chemical inhibitors, our laboratory discovered that *Chlamydia* specifically recruits transferrin-containing vesicles from the slow-recycling endocytic pathway (37). Once delivered into the inclusion, iron is likely imported into bacteria through an ABC transporter system, encoded by *ytgABCD*, which is the only known iron acquisition system in *Chlamydia* species (39–41). The C-terminus of the YtgC permease, referred to as YtgR, is homologous to the *Cornyebacterium* repressor DtxR, and has been recently characterized as an iron-dependent repressor of the *ytgABCD* iron-acquisition operon (41). A recent review highlights the differences between iron-acquisition strategies of *Chlamydia* with other intracellular bacteria (26).

Conversion to the aberrant phenotype in response to iron-starvation reduces the infectious potential of *Chlamydia*, since only a portion of RBs recover from stress and complete development into infectious EBs once iron is added back into the media (42). Previous studies have characterized aberrant *C. trachomatis* after long-term treatment with the iron-chelator deferoxamine, and have detected increased expression of the iron-binding protein YtgA, indicating its role in iron-uptake (40, 43, 44). However, these studies added deferoxamine at the time of infection, and did not monitor transcriptional or proteomic patterns until ≥24 hours post-infection, making it difficult to determine if this up-regulation is part of the initial response to iron starvation. Immediate genome-wide transcriptional responses to iron limitation have not yet been characterized in detail, leaving a gap in the current knowledge of how *Chlamydia* regulates its response to changes in iron availability.

This study provides the first global profile of the *C. trachomatis* transcriptional response to iron starvation. Our short-term, effective treatment regimen in combination with deep RNA-sequencing reveals the immediate response of *Chlamydia* to iron-starvation in the logarithmic phase of growth when the bacteria are in the RB form. Here we utilize this dataset to map the specific biological pathways altered in response to iron-starvation. Taken together our results provide important clues to how *Chlamydia* survives iron limitation. Accumulation of metabolite precursors is prioritized over macromolecular biosynthesis. In addition, the transcriptional induction of genes involved in adaptation to other stress, e.g. oxidative stress and amino acid starvation, points to the inability of *Chlamydia* to tailor its transcriptional response to a specific stress. Lastly,

the global transcriptomic profile of iron-starved *Chlamydia* provided valuable insights into how the biphasic developmental cycle might irreversibly switch to persistence.

RESULTS

Treatment optimization to detect the immediate chlamydial response to iron-starvation

The bivalent chelator 2,2-Bipyridyl (BPDL) has been shown to deplete both ferrous and ferric iron from *Chlamydia*-infected cells during long-term treatment, and it induces the development of aberrant forms more consistently and homogenously than the previously used ferric iron chelator, deferoxamine (42). Here, we determined the optimal duration of BPDL treatment to induce iron-responsive transcription without inducing morphological abnormalities in *Chlamydia*. We chose to begin starvation during mid-cycle development (12h p.i.) instead of at the beginning of infection for two reasons: 1) to test the response of actively replicating *Chlamydia* that are able to maximally respond to stress, and 2) to ensure that both treated and mock-treated *Chlamydia* remain in the same stage of development (RB). We monitored chlamydial morphology, growth, and transcriptional responses after 3, 6, and 12h of BPDL treatment (Figure 1A). Indirect immunofluorescent confocal microscopy revealed similar morphology between mock-treated and BPDL-treated forms for up to 12h of BPDL-treatment (Figure 1B). Interestingly, observation of BPDL-treated cultures by light microscopy revealed an obvious decrease in Brownian movement within inclusions after 6 or more hours of treatment (data not shown). This observation is consistent with our findings that

chlamydial growth is reduced compared to mock-treated after only 6h of BPDL-treatment, as determined by quantitative PCR of chlamydial genomes (Figure 1C).

We monitored the transcriptional response of the known iron-responsive genes *ytgA* and *ahpC* by reverse transcriptase quantitative polymerase chain reaction (RT-qPCR) to validate the iron starvation protocol (39, 40, 42, 45). Elevated transcription of both iron-starvation markers was detected after only 6h BPDL-treatment, compared to mock-treated (1.5-fold and 1.7-fold). Maximum differences in transcription of both markers were detected after 12h of BPDL treatment (2.8-fold and 3.7-fold; Figure 1D). In the same experiment, we also monitored the transcriptional profile of the early gene, *euo*, which decreases during late stages of normal development. Multiple persistence models have demonstrated dysregulated of *euo* transcription, with high levels of *euo* mRNA detected late in development under persistence-inducing conditions (14, 42, 44). After 12h BPDL treatment, we observed that *euo* transcript levels remained elevated relative to the mock-treated control, indicating dysregulated transcription or a possible delay in development (Figure 1E, top). This delay in development during longer BPDL-treatment is supported by the lack of recoverable inclusion-forming units (IFUs) detected after 12 or 24h BPDL-treatment compared to mock-treated controls (Figure 1F), indicating a possible lack of RB-to-EB differentiation. Because 6h BPDL-treatment is sufficient to induce iron-responsive transcription without inducing the morphology and transcriptional pattern associated with persistence, we chose it as the optimal duration of iron-starvation for our genome-wide transcriptional studies. We also included 3h

BPDL-treatment to detect the earliest possible response to iron-starvation prior to BPDL-induced changes in growth.

Global transcriptional response of *C. trachomatis* to iron-starvation during mid-cycle development

The primary global response of *C. trachomatis* to mid-cycle iron starvation was determined by RNA-sequencing (RNA-seq). We utilized an Ion Proton for sequencing, which allowed for easy and rapid scaling of timepoints based on observed yield of mapped reads. This approach is relevant to the study of *Chlamydia* transcription because chlamydial mRNA represents a small proportion of the total RNA at the time points analyzed, even after significant enrichment steps. For mid-cycle iron starvation studies, we aimed for greater than 10x coverage of 100% of the *C. trachomatis* genome, with a minimum of 3 biological replicates per sample. The sequencing reads were trimmed to exclude adaptor sequences and polyclonal reads, followed by exclusion of reads less than 30 nucleotides in length. The remaining reads were aligned to the *C. trachomatis* genome and plasmid, with 2 to 23% of trimmed reads mapping. Average read lengths varied from 92 to 134 nucleotides, requiring an average of 108,837 mapped reads to reach our coverage goal. A summary of the read and mapping statistics for all of our samples can be found in Table 1. Alignments, comparisons, and normalization of aligned reads were done with CLC Genomics Workbench version 9.0 according to default settings. All mid-cycle conditions (12h untreated, 12+3h BPDL, 12+3h mock, 12h+6h BPDL, 12+6h mock) were compared using the CLC Genomics experiment tool, normalized by quantile scaling and analyzed

for differential gene expression using EdgeR statistical analysis with false-discovery rate (FDR) calculation. Because we included ribosomal rRNA, eukaryotic mRNA, and small RNA (<100 nt) depletion steps when preparing chlamydial mRNA for RNA-seq, we also excluded tRNAs, rRNAs, and genes with < 10 mean reads in a sample group prior to normalization and analysis.

The genome-wide profile of mock-treated and BPDL-treated gene expression during mid-cycle development (12h to 18h post-infection) is displayed as a heatmap of normalized expression values (Figure 2A). Mock-treated (left) and BPDL-treated (right) profiles are remarkably similar across all genes that significantly change during normal mid-cycle development of *Chlamydia* (based on comparisons 12h vs 15h, 15h vs 18h, or 12h vs 18h, p-value ≤ 0.01). The annotated expression heatmap and EdgeR comparisons for normal growth can be found in Supplemental Figure 1 and Supplemental Table 1, respectively. The entire RNA-seq dataset of normal development can be found in Supplemental Table 2. The similarity between global expression profiles indicates that *Chlamydia's* normal development is not dysregulated after only 3h or 6h of BPDL-treatment. However, EdgeR analysis of BPDL-treated cultures compared to mock-treated samples (at equivalent time points post-infection) revealed 8% (76/889) of the genome was differentially expressed after 3h BPDL–treatment and 1% (12/889) was differentially expressed after 6h BPDL-treatment. Genes that were differentially expressed with a maximum p-value of 0.01 are displayed in a heatmap of fold-change differences between BPDL-treated and mock-treated samples (Figure 2B). Examples of decreased transcription after 3h and 6h BPDL-treatment include the ribosomal subunit

243 genes *rpsO* and *rpsT*, and the type III secretion genes *copB* and *scc2*, respectively.
244 Transcription of the tryptophan salvage pathway operon, *trpBA,* and the ribonucleotide
245 reductase operon, *nrdAB,* was significantly increased after both 3 and 6h of treatment.
246 Iron-responsive genes that were differentially expressed with a p-value $\leq$ 0.01 after 3 or
247 6h of BPDL-treatment are listed in Table 2 and Table 3, respectively. The fully
248 annotated heatmap can be found in Supplemental Figure 2, and the full set of RNA-
249 sequencing results for mid-cycle iron starvation can be found in Supplemental Table 3.
250
251 **Functional categorization of differentially expressed genes during mid-cycle**
252 **response to iron-starvation.**
253 Annotations and functional categories of differentially expressed genes during mid-
254 cycle iron-starvation were retrieved from UniProt and are listed in Table 2 and Table 3.
255 Genes differentially expressed, with a minimum p-value of 0.01, after only 3h of BPDL-
256 treatment are grouped by functional category of induced and reduced transcripts (Table
257 2, Figure 3) (46). Of the 39 genes significantly induced after only 3h iron-starvation,
258 representing 4% of the genome, five categories were equally represented with 3 genes
259 each: energy metabolism (*glgA, lpdA, glmS*), amino acid biosynthesis (*trpA, trpB, aroL*),
260 DNA replication and repair (*nrdA, recA, dnaQ*), type III secretion (*mcsC, ctl0085,*
261 *ctl0043*), and translation (*pheT, cysS, thrS*). Of the 37 genes that were significantly
262 reduced in response to 3h BPDL-treatment, representing 4% of the genome, the
263 majority of these (39%) are associated with translation (*prfA, rplW, rsfS, smpB, ctl0132,*
264 *rpsK, rplT, rplN, ctl0680, rpmI, rmpJ, infa2, rpsT, rpsO*), and 11% are associated with
265 nutrient transport (*ctl0061, ctl0485, gltT,* and *ytgD*). Transcript levels of only 5 genes

were significantly increased after 6h BPDL-treatment (*trpB, trpA, nrdA, ctl0071,* and *nrdB*) while transcript levels of 7 genes were decreased (*ctl0185, ctl0619, tsp,* and the entire *scc2-ctl0840-cobB-copD* operon) (Table 3).

To independently confirm the mid-cycle response detected by RNA-sequencing, we utilized RT-qPCR. Increased transcription in response to iron-starvation was confirmed for all of the transcripts tested by RT-qPCR, with the exception of *recA* (Figure 4A). None of the tested down-regulated genes were significantly reduced compared to controls by RT-qPCR, likely due to the fact that the genes tested were very low in abundance at the timepoints tested (Figure 4B).

Functional categorization of differentially expressed genes during early-cycle response to iron-starvation.

Chlamydia infections of the genital tract are asynchronous. Thus *Chlamydia* could be exposed to host-induced stress at any point in the developmental cycle. For this reason, we extended our analysis of the immediate response to iron starvation to an earlier point in the developmental cycle. *Chlamydia*-infected cells were treated with BPDL starting at 6h post-infection, which is after the initial EB-to-RB differentiation and at the beginning of the logarithmic growth phase. RNA and genomic DNA were collected at 9h post-infection for both treated and mock-treated samples. RNA-seq and alignments were performed as described above. A summary of mapped reads and coverage can be found in Table 1.

289 Genes differentially expressed during the early cycle response (6+3h BPDL vs 6+3h
290 mock-treated), with a maximum p-value of 0.01, are grouped by functional categories of
291 induced and reduced transcripts (Figure 5). The full set of differentially expressed genes
292 and their annotations can be found in Table 4. Similar to results of the mid-cycle
293 response, transcription of 4% of the genome was induced, including genes involved in
294 DNA replication and repair (*nrdA, nrdB, mutS, dnaQ,* and *recA*), amino acid
295 biosynthesis (*trpB, trpA*, *aspC_1*, and *glyA*), and translation (*ctl0111*, *trpS*, *thrS*, and
296 *aspS*) during the early-cycle response to iron starvation. Uniquely, genes involved in
297 redox homeostasis (*pdi*, *ahpC* and *sodM*) were also up-regulated in response to iron-
298 starvation starting at 6h post-infection but not during the mid-cycle response. Of the 23
299 genes with reduced transcription during the early-cycle response to iron-starvation (3%
300 of the genome), 17% are associated with translation (*rplW, prfA, rplC, ftsY*), and 13%
301 with DNA replication and repair (*pGP8D*, *amn*, and *dnaX_1*).
302
303 Up-regulation of *trpA* transcription during early-cycle iron-starvation was confirmed
304 by RT-qPCR, while only modest increases were observed for the other up-regulated
305 genes tested (Figure 6A). Down-regulation of *ctl0430*, *ctl0063,* and *incD* during iron-
306 starvation could not be confirmed by RT-qPCR (Figure 6B). We reasoned that early-
307 cycle responses were not detected by RT-qPCR for most of our tested genes due to the
308 limit of detection of the technique. The raw values detected for most of our early-cycle
309 transcripts fell at or below the lowest concentrations of our standard curves. Between 6
310 and 9h post-infection, chlamydial mRNA represents a very small proportion of the total
311 RNA. This limitation was overcome for RNA-seq experiments by depleting rRNAs and

312 eukaryotic RNA prior to synthesizing cDNA. However, cDNA used in RT-qPCR was
313 prepared from total RNA. The overwhelming proportion of eukaryotic RNA present in
314 the undiluted cDNA used as template may have impeded accurate detection of
315 transcripts.
316
317 **Network and biological pathway analysis**
318 To further analyze the relevance of these gene expression changes to chlamydial
319 survival, we utilized the bioinformatics tool STRING-db v.10.5 to generate networks of
320 functionally associated genes (47). Representation of differentially expressed gene sets
321 (p-value ≤ 0.05) from short-term iron starvation (3h) reveals gene networks with
322 intersecting pathway clusters (manually added grey circles). Consistent with our
323 predicted functional categories, network analysis of both early (Figure 7A) and mid-
324 cycle (Figure 7B) responses to iron-starvation revealed clusters that include amino acid
325 biosynthesis, DNA replication and repair, and translation. Functional clustering of the
326 mid-cycle response also revealed the entire cluster of genes necessary to convert
327 pyruvate to acetyl-CoA, as well as gene clusters involved in tRNA modification and
328 charging.
329
330 The locus identifiers of genes in each identified cluster were submitted to
331 KEGGMapper v2.8 to determine possible roles in specific biological pathways (48). For
332 example, genes from the early-cycle DNA replication and repair cluster (Figure 7A)
333 were mapped to multiple pathways including purine metabolism (5), pyrimidine

metabolism (5), mismatch repair (5), replication (4), homologous recombination (3), double-stranded breaks repair (2), and base excision repair (1).

Nucleotide metabolism

We modified the KEGGMapper output for pyrimidine metabolism to indicate the direction of change in mid-cycle gene expression during iron starvation (Figure 7C). Under all iron-starvation conditions, the ribonucleotide reductase genes *nrdA* and *nrdB* were up-regulated. Ribonucleotide diphosphates (NDPs) bound to NrdA are converted by NrdB to deoxynucleotide diphosphates (dNDPs). These dNDPs are not likely further converted to dNTPs, as indicated by the down-regulation of nucleotide diphosphate kinase, *ndk*. Expression of thymidylate synthase gene, *thyX*, which converts dUMP to dTMP, was also up-regulated during iron starvation. Available dUMP would likely be derived from the UDP pool, instead of from the dUTP pool, since transcription of the dUTP pyrophosphatase gene, *dut*, is down-regulated during iron-starvation. Taken together, these transcriptional changes would result in a net increase in dNDPs, enabling rapid DNA replication when iron levels and *ndk* expression return to normal (Figure 7C).

Amino acid biosynthesis

Functional clustering also indicates that *Chlamydia* prioritizes maintenance of amino acid pools during iron starvation. Multiple amino acid synthesis, inter-conversion, and uptake mechanisms were up-regulated in response to short-term iron-starvation. Transcriptional up-regulation of the branched chain amino acid transporter, *brnQ,* the

aspartate aminotransferase, *aspC*, and the serine hydroxymethyltransferase, *glyA* may increase the diversity of the amino acid pool such that *Chlamydia* can quickly adapt to fluctuations in amino acids. Surprisingly, the tryptophan salvage pathway genes, *trpB* and *trpA,* were consistently up-regulated during short-term iron-starvation. The tryptophan synthase subunit TrpB catalyzes the beta-replacement of indole with serine to form tryptophan (Trp), while TrpA facilitates the interaction of TrpB with indole (49). Their role in recovery from IFN-g and Trp-starvation stresses is well documented, but differential regulation in response to iron-starvation is novel (50, 51). While the biological relevance of *trpBA* induction during iron-starvation is unclear, we reason that *Chlamydia* could in fact prepare for further immune insult (e.g. IFN-g induction of indoleamine 2,3-dioxygenase expression) by increasing intracellular Trp levels. Taken together, iron-starvation may increase levels of serine, aspartate, glutamate, branched-chain amino acids, and tryptophan, many of which are essential for normal development (52–56). Amino acid biosynthetic genes were significantly overrepresented (4.38-fold, p-value=0.0464) in the set of differentially expressed mid-cycle genes as determined by the Panther Overexpression Test (57).

Translation

The largest cluster generated from STRING-db included translation factors of the mid-cycle response (Figure 7B). Based on protein annotations in Uniprot and Biocyc databases, it is evident that *C. trachomatis* responds to iron-starvation by shutting down factors involved in every step of translation: ribosome assembly, initiation, elongation, termination, ribosome recycling, and peptide targeting (46, 54; Table 4). While

preventing the assembly and function of translational machinery, *Chlamydia* also responds to iron starvation by increasing factors important for synthesis and modification of tRNAs, in addition to increasing transcription of *rnC,* the product of which cleaves rRNA transcripts into ribosomal subunit precursors (Table 4). Collectively, these findings indicate that *Chlamydia* responds to iron starvation by shutting down production of new proteins, effectively preventing progression of the developmental cycle. However, *Chlamydia* likely prioritizes maintenance of an amino-acyl-tRNA pool and ribosomal precursors such that translation can rapidly resume under better environmental conditions. Translation genes were significantly overrepresented (3.26-fold, p-value=0.0243) in the set of mid-cycle differentially expressed genes as determined by the Panther Overexpression Test (57).

Acetyl-coA synthesis

Transcription of the entire set of genes necessary for conversion of pyruvate to acetyl-CoA was induced during the mid-cycle response to BPDL-treatment (Figure 7D). This includes the lipoylation enzymes *lipA* and *lpdA,* and the entire pyruvate dehydrogenase complex, *pdhABC*. In addition, transcription of the TCA cycle gene *mdhC* and glycolysis gene *eno* was induced, likely driving formation of pyruvate from different carbon sources. Acetyl-CoA can be converted to malonyl-CoA for fatty-acid biosynthesis or utilized in the formation of N-acetylglucosamine-1-phosphate for peptidoglycan synthesis, both of which are required for rapid growth of *Chlamydia* (59, 60). Since transcription of the peptidoglycan-modifying enzymes, *glmS* and *murB,* were also increased during iron starvation, acetyl-coA is likely used to form new

403 peptidoglycan. Expression of fatty acid synthesis genes was unchanged during iron-
404 starvation.
405
406 DISCUSSION
407 We monitored the immediate global transcriptional response of *Chlamydia*
408 *trachomatis* serovar L2 to short-term iron-starvation during early and mid-cycle (RB
409 phase) development. In contrast to previous studies of iron starvation in *Chlamydia*, our
410 short-term treatment with BPDL did not cause the hallmark changes in morphology and
411 *euo* transcription associated with persistence. This approach enabled us to detect a
412 response specific to iron starvation as *Chlamydia* tries to adapt to stress, rather than the
413 transcriptome of the aberrant bacterium. By deep RNA-sequencing we were able to
414 identify novel primary transcriptional responses, representing 7-8% of the genome, after
415 only 3h of iron-starvation with BPDL. It is possible that a more immediate response
416 could be detected with even shorter BPDL treatments, though we expect a longer
417 duration is required to chelate both free iron and iron bound to protein complexes in
418 intracellular *Chlamydia*. Since only 12 genes were differentially expressed after 6h
419 BPDL-treatment, a longer duration of treatment may be necessary to detect the full
420 secondary response, which may not be obvious until the effects of the primary
421 transcriptional response are realized at the protein level. This is supported by the fact
422 that 6h BPDL-treatment maintains induction of the primary response operons, *trpBA*
423 and *nrdAB,* while reducing or delaying expression of some late cycle genes (*scc2-*
424 *ctl0840-copB-copD, tsp*). Decreased or delayed late gene expression has also been
425 observed during long-term iron-starvation (42, 45, 61, 62).

In agreement with proteomic observations of deferoxamine-treated *C. trachomatis* after 24h and *C. pnuemoniae* after 48h post-infection, we observed up-regulation of *ctl0874*/*cadd*, *ahpC, eno, and htrA* during short-term BPDL-treatment (44, 63). In contrast to previous iron-starvation studies, we did not detect a significant increase in *ytgA* expression in our RNA-seq results. We expected the *ytgABCD* iron acquisition operon to be immediately induced in response to iron-starvation, since its repression by YtgR is dependent on available iron (41). Expression of the *ytgABCD* operon peaks during mid-cycle development, indicating that the iron-dependent repressor, YtgR, may be inactive or at low levels during early and mid-cycle (14, 41). It is possible that we do not observe significant differences in the expression of the operon during iron-starvation because it is already maximally expressed in the mock-treated controls (Table S2). Global detection of YtgR repression by CHIP-sequencing or targeted analysis of specific promoters will be necessary to delineate the contribution of YtgR activity to the detected iron-responsive regulon. Additionally, other unidentified iron-uptake and iron-dependent repression mechanisms may exist, and thus could be represented in our set of iron-starvation induced genes.

Consistent transcriptional induction of the ribonucleotide reductase genes, *nrdA* and *nrdB,* under short-term iron starvation, indicates that deoxynucleotides may be important to survive this stress. However, since NrdB requires iron for its function, deoxynucleotide levels may not increase until iron becomes available. Instead, high levels of inactive NrdA-B complexes may actually impede replication and development

448 by inducing stalling at replication forks, providing a possible explanation for the
449 decreased replication observed during iron-starvation (77, 79).
450
451 *Chlamydia's* immediate transcriptional response to iron-starvation is remarkably
452 similar to stringent responses in other bacteria, which enable rapid adaptation to various
453 stresses by diverting resources from macromolecular biosynthesis, e.g. translation, and
454 growth to immediate survival, often resulting in a quiescent state (64, 65). This rapid
455 transcriptional response is achieved through synthesis of the chemical alarmone,
456 (p)ppGpp, which interacts with RNA polymerase and DksA to globally modify
457 transcriptional activity (66, 67). During amino acid starvation in bacteria, uncharged
458 tRNAs in the A-site of ribosomes are sensed by RelA, which responds by synthesizing
459 (p)ppGpp from ATP and GDP or GTP (68, 69). (p)ppGpp can also be synthesized and
460 hydrolyzed by SpoT during other stress conditions. However, since *Chlamydia* lacks the
461 RelA and SpoT homologues necessary for (p)ppGpp synthesis, they likely evolved
462 alternative mechanisms to reduce growth and increase survival responses during stress
463 (16, 70, 71). It is hypothesized that IFN-gamma induced depletion of tryptophan leads
464 to ribosome stalling at tryptophan codons, and differences in tryptophan codon content
465 may directly regulate translation efficiency and mRNA stability (16, 71–73). *Chlamydia*
466 may have adapted the tryptophan-content of open-reading frames (ORFs) to guide the
467 stress response during tryptophan-depletion. Trp-poor ORFs which may be important
468 for immediate survival of stress, such as menaquinone biosynthesis enzymes, would be
469 translated more efficiently during tryptophan-depleted conditions than Trp-rich ORFs,

such as nutrient transporters, which are more important for supporting rapid growth during improved conditions (73).

Pathway analysis clearly indicates that transcripts involved in all steps of translation from initiation to ribosome recycling are down-regulated during iron-starvation. This reduction in translation factors may lead to an eventual shutdown or modification of translation activity that could increase survival during stress. By shutting down energy expensive protein synthesis, ATP and GTP pools can be rerouted to immediate survival responses (tRNA-charging, transcription). Similarly, iron-starvation reduces the transcription of several ABC transporter genes, which require ATP for their function. Uncoupled RNA and protein levels in *Chlamydia* have also been observed during IFN-g stress (16). The apparent decrease in translation during IFN-gamma exposure could be exacerbated by decreases in the levels of components of the translation machinery in response to simultaneous iron-starvation. However, decreased expression of translation factors during the primary response to iron-starvation may not be apparent until pre-existing ribosomal-protein complexes are degraded or destabilized. This may explain why ≥24h of iron-starvation is required to induce the development of aberrant RBs (42). Down-regulation of translation factors during iron starvation will have to be examined at the protein level to determine its contribution to adaptation to iron starvation and development of persistence.

In contrast to down-regulation of translation, iron starvation increases transcription of amino-acyl synthesis genes (*cysS, pheT, glyQ, aspS, thrS*), which are responsible for

493 charging tRNAs with amino acids. The apparent disconnect between increased amino-
494 acyl-tRNA pools and decreased translation indicates possible survival mechanisms.
495 Charged tRNAs might be utilized in an immediate survival response to iron-starvation,
496 prior to the turnover of ribosomal subunits. Alternatively, *Chlamydia* may be
497 accumulating charged tRNAs for recovery and resumption of development when normal
498 levels of iron and translation factors are restored.
499
500 Multiple amino acid synthesis, inter-conversion, and uptake mechanisms were up-
501 regulated in response to short-term iron starvation. Surprisingly, the primary response
502 includes an increase in transcripts involved in tryptophan salvage, *trpB* and *trpA*, but not
503 the tryptophan-dependent repressor *trpR*. TrpR-dependent regulation of *trpRBA*
504 transcription has been extensively studied during tryptophan starvation and IFN-g
505 treatment, but rarely, if ever, in the context of iron-starvation (50, 74, 75). Notably, *trpB*,
506 but not *trpR* levels were also increased under estradiol-induced persistence, suggesting
507 a *trpR*-independent mechanism of inducing tryptophan salvage transcription may exist
508 (76).
509
510 A major theme that emerged from our gene expression analysis is that *Chlamydia*
511 likely perceives iron starvation as a signal to prepare for further nutrient deprivation and
512 immune insult. Transcriptional up-regulation of tryptophan salvage pathway (trpB, trpA),
513 oxidative stress (*ahpC*, *pdi,* and *sodM*) and DNA repair (*mutS, mutL, ssb, ung, recA*)
514 genes indicate a protective response against antimicrobial insults of the inflammatory
515 immune response (e.g. IDO activation, reactive oxygen species). As an obligate

intracellular pathogen, *Chlamydia* has undergone reductive evolution with constant selective pressure from the host immune system and its multiple anti-chlamydial effectors. Due to its small genome (~ 1 Mbp), *Chlamydia* may not have the capability to induce a specific transcriptional response to each particular stressor, and the simultaneous deployment of stress responses may have been the most parsimonious route of adaptation to immune insult. In this case, we would expect that iron-starved *Chlamydia* would be better protected from damage by antimicrobial insults than mock-treated *Chlamydia*. Immediate transcriptional responses to other stress conditions will need to be monitored to determine if this coordination of antimicrobial responses is unique to iron starvation.

This study provides the first evidence of an iron-dependent regulon for *C. trachomatis*. By using a systems-approach to delineate *Chlamydia*'s transcriptional response to iron starvation, we have been able to detect biological pathways and place them in the context of chlamydial development. These findings are novel, and add to previous studies of iron-dependent transcriptional and proteomic profiling in aberrant RBs, revealing transcriptional adaptive strategies prior to the development of a persistent state. Additionally, our results include a high-resolution profile of mid-cycle development of *C. trachomatis* serovar L2, including relevant time points for monitoring shifts in early, mid, and late-cycle gene expression. We expect this dataset will prove useful for future studies that seek to determine *Chlamydia*'s immediate transcriptional response to other chemical and/or nutrient stresses. Our findings include previously unrecognized shifts in energy utilization and down-regulation of translation that

resemble a stringent-like survival response. *Chlamydia* may utilize a two-stage approach of increasing transcription of survival genes in the short term to delay development and survive during iron-starvation, followed by an eventual shutdown of translation at later times of sustained stress. The latter might account for the observed irreversibility of the persistent state during long-term starvation for iron or tryptophan.

MATERIALS AND METHODS

Cell Culture and infection

HeLa monolayers were infected with *C. trachomatis* strain L2 434/Bu in 6-well plates at a multiplicity of infection (MOI) of 2 for RNA and gDNA collection experiments, and on coverslips in 24-well plates for morphology studies. Cells were grown in DMEM supplemented with 10% FBS, 2 mM glutamine, and 10 micrograms/mL gentamycin in 5% CO_2 at 37° C. HeLa cells used in this study were started from P1 stocks from ATCC, and were regularly checked for contamination by DAPI-staining and the Universal Mycoplasma detection kit (ATCC).

RNA-sequencing

RNA was collected and pooled from 2 or 4 T75 flasks of *C. trachomatis*-infected HeLa monolayers that had been treated with 100 µM 2,2-Bipyridyl (BPDL) starting at 6 or 12h hours post-infection (6h + 3h BPDL, 12h + 3h BPDL, 12h + 6h BPDL) and in mock-treated samples at equivalent timepoints post-infection (9h, 12h, 15h, 18h). RNA was purified using the RiboPure Bacteria (Ambion) kit as per manufacturers instructions. Total RNA was further enriched for transcripts over 100 nucleotides in length with the

562 MegaClear kit (Ambion). Mammalian transcripts and rRNAs were removed with the
563 MicrobEnrich kit (Ambion) and bacterial rRNAs were removed using the MicrobExpress
564 kit (Ambion), repeating 2-3 times. The integrity and quantity of total and depleted RNA
565 was monitored with an AATI Fragment Analyzer. cDNA libraries were prepared with the
566 Ion Total RNA-seq Kit V2, and sequencing beads prepared using an ion Chef, and
567 sequencing performed on an Ion Proton chip with HiQ chemistry. Primary sequence
568 analysis, trimming, and binning of reads was performed using Torrent Suite Software
569 version 5.0.5. Remaining reads were mapped to the combined core genome of *C.*
570 *trachomatis* strain L2 434/Bu (Genbank Accession: AM884176) and the plasmid of *C.*
571 *trachomatis* L2b CS784/08 (NZ_CP009926) using CLC Genomics Workbench 9,
572 requiring reads be at least 30 nucleotides in length, with default alignment parameters.
573
574 The EdgeR algorithm in CLC Genomics was used to determine differential gene
575 expression during development and iron-starvation, assuming a false-discovery rate of
576 10% and p-values ≤ 0.05. tRNAs and ribosomal RNAs were filtered from the reads to
577 account for differences in depletion efficiency, and only genes with at least 5 mapped
578 reads were included in the analysis. Differentially expressed genes were confirmed for
579 selected transcripts by RT-qPCR.
580
581 **qPCR and RT-qPCR**
582 *C. trachomatis*-infected HeLa monolayers were treated with 100 micromolar BPDL
583 starting at 6 or 12h hours post-infection (6h + 3h BPDL, 12h + 3h BPDL, 12h + 6h
584 BPDL) and mock-treated samples at equivalent timepoints post-infection (6h, 9h, 12h,

15h, 18h). RNA and genomic DNA (gDNA) were collected with the RiboPure Bacteria and the DNeasy Blood and Tissue (Qiagen) kits, respectively. cDNA was generated with Superscript IV reverse transcriptase (Life Technologies) from 200-500 nanograms RNA as per manufacturer's instruction, except the use of random nonamers instead of hexamers. Transcripts were amplified with PowerUp SYBR Green system from undiluted cDNA for early (6-9h) or diluted 1:10 in 10 mM Tris for midcycle (12-18h) samples and detected with Applied Biosystems 7300 RT-qPCR system.

Chlamydial morphology

Chlamydiae were monitored for changes in morphology in response to mock-treatment or treatment with 100 micromolar BPDL starting at 12h post-infection for 3, 6, or 12h. Infected cultures were fixed on coverslips and stained with pooled human serum at 1:750, followed by goat-anti-human antibody conjugated to Alexa Fluor 488 (ThermoFisher) at 1:1000. DNA was stained with DAPI at 5 micrograms/mL. Images were taken on a Leica SP8 confocal microscope with a 63X oil-objective and 4X zoom.

IFU assay

Chlamydiae were monitored for changes in infectivity in response to mock-treatment or treatment with 100 micromolar BPDL starting at 12h post-infection for 12 or 24h, at an MOI of 1. Infected cultures were scraped into 300 microliters SPG and stored at -80 C for later testing. Thawed lysates were serially diluted into complete DMEM, centrifuged onto HeLa monolayers in 24-well plates, washed with HBSS, and allowed to infect for 24h. Infected cultures were fixed and stained with pooled human serum at 1:750,

608 followed by goat-anti-human antibody conjugated to Alexa Fluor 488 (ThermoFisher) at
609 1:1000. Inclusions were counted by fluorescent microscopy and inclusion-forming units
610 (IFU) were calculated as previously described.
611
612 **Visual analysis of differentially expressed genes**
613 Functional categories were assigned for all genes differentially regulated with a p-value
614 ≤ 0.01 by referring to the GO terms listed on UniProt. Pie charts were generated using
615 the “pie” function in Rstudio. Heatmaps were generated in Rstudio using the package
616 “pheatmaps”, with parameters set to average clustering and Euclidean distance. The
617 Panther overexpression test in Panther v12.0 was done on differentially regulated gene
618 sets (total) with p-values ≤ 0.01, using the default parameters and Bonferri correction.
619 Pathway analysis was performed on differentially regulated genesets with p-values ≤
620 0.05 with STRING-db v.10.5 set to confidence ≥ 0.7. StringDB maps were slightly
621 modified to make space for pathway labels, without altering network relationships.
622 Clustered genes detected with StringDB were further analyzed using KeggMapper
623 v.2.8, and pathway maps were generated based on KeggMapper output using Affinity
624 Designer v1.4.1.
625
626 **Data availability**
627 Raw and processed sequencing files were submitted to the NCBI Gene Expression
628 Omnibus (GEO) as a Superseries, and the mid-cycle and early-cycle projects can be
629 found using accession number GSE106763.
630

ACKNOWLEGEMENTS

We would like to acknowledge Dr. Scot Ouellette and Nicholas Pokorzynski for critical reading of the manuscript. This work was funded by start-up funds for R.A.C. from the School of Molecular Biosciences, College of Veterinary Medicine at Washington State University, NIH grant 2R01AI065545-06A1 awarded to R.A.C., and NIH training grant T32AI7025-36 for A.J.B.

REFERENCES

1. **CDC. 2016. Sexually Transmitted Disease Surveillance.** 2015. Atlanta: U.S. Department of Health and Human Services.
2. **Price MJ, Ades AE, Welton NJ, Simms I, Macleod J, Horner PJ.** 2016. proportion of pelvic inflammatory disease cases caused by *Chlamydia trachomatis*: consistent picture from different methods. J Infect Dis **214**:617–24.
3. **Kjaer HO, Dimcevski G, Hoff G, Olesen F, Ostergaard L**. 2000. Recurrence of urogenital *Chlamydia trachomatis* infection evaluated by mailed samples obtained at home: 24 weeks' prospective follow up study. Sex Transm Infect **76**:169–72.
4. **Batteiger BE, Tu W, Ofner S, Van Der Pol B, Stothard DR, Orr DP, Katz BP, Fortenberry JD. 2010.** Repeated *Chlamydia trachomatis* genital infections in adolescent women. J Infect Dis **201**:42–51.
5. **Wyrick PB. 2010.** *Chlamydia trachomatis* persistence *in vitro*: an overview. J Infect Dis **201**:88–95.
6. **Lewis ME, Belland RJ, AbdelRahman YM, Beatty WL, Aiyar AA, Zea AH, Greene SJ, Marrero L, Buckner LR, Tate DJ, McGowin CL, Kozlowski PA,**

O'Brien M, Lillis RA, Martin DH, Quayle AJ. 2014. Morphologic and molecular evaluation of *Chlamydia trachomatis* growth in human endocervix reveals distinct growth patterns. Front Cell Infect Microbiol **4**:71.

7. **AbdelRahman YM, Belland RJ.** 2005. The chlamydial developmental cycle. FEMS Microbiol Rev **29**:949–959.

8. **Matsumoto A, Manire GP.** 1970. Electron microscopic observations on the effects of penicillin on the morphology of *Chlamydia psittaci*. J Bacteriol **101**:278–85.

9. **Kazar J, Gillmore JD, Gordon FB.** 1971. Effect of Interferon and Interferon Inducers on Infections with a nonviral intracellular microorganism, *Chlamydia trachomatis*. Infect Immun **3**:825–32.

10. **Raulston JE.** 1997. Response of *Chlamydia trachomatis* serovar E to iron restriction *in vitro* and evidence for iron-regulated chlamydial proteins. Infect Immun **65**:4539–47.

11. **Byrne GI, Lehmann LK, Landry GJ.** 1986. Induction of tryptophan catabolism is the mechanism for gamma-interferon-mediated inhibition of intracellular *Chlamydia psittaci* replication in T24 cells. Infect Immun **53**:347–51.

12. **Beatty WL, Byrne GI, Morrison RP.** 1993. Morphologic and antigenic characterization of interferon gamma-mediated persistent *Chlamydia trachomatis* infection *in vitro*. Proc Natl Acad Sci U S A **90**:3998–4002.

13. **Beatty WL, Morrison RP, Byrne GI.** 1995. Reactivation of persistent *Chlamydia trachomatis* infection in cell culture. Infect Immun **63**:199–205.

14. **Belland RJ, Nelson DE, Virok D, Crane DD, Hogan D, Sturdevant D, Beatty**

WL, Caldwell HD. 2003. Transcriptome analysis of chlamydial growth during IFN- -mediated persistence and reactivation. Proc Natl Acad Sci **100**:15971–15976.

15. **Reveneau N, Crane DD, Fischer E, Caldwell HD.** 2005. Bactericidal activity of first-choice antibiotics against gamma interferon-induced persistent infection of human epithelial cells by *Chlamydia trachomatis*. Antimicrob Agents Chemother **49**:1787–93.

16. **Ouellette SP, Hatch TP, AbdelRahman YM, Rose LA, Belland RJ, Byrne GI.** 2006. Global transcriptional upregulation in the absence of increased translation in *Chlamydia* during IFNgamma-mediated host cell tryptophan starvation. Mol Microbiol **62**:1387–401.

17. **Stephens RS, Kalman S, Lammel C, Fan J, Marathe R, Aravind L, Mitchell W, Olinger L, Tatusov RL, Zhao Q, Koonin E V.**, Davis RW. 1998. Genome Sequence of an Obligate Intracellular Pathogen of Humans: *Chlamydia trachomatis*. Science **282**:754-9.

18. **Chen W.** 2011. IDO: more than an enzyme. Nat Immunol **12**:809–811.

19. **Byrd TF, Horwitz MA.** 1989. Interferon gamma-activated human monocytes downregulate transferrin receptors and inhibit the intracellular multiplication of *Legionella pneumophila* by limiting the availability of iron. J Clin Invest **83**:1457–1465.

20. **Nemeth E, Valore E V, Territo M, Schiller G, Lichtenstein A, Ganz T.** 2003. Hepcidin, a putative mediator of anemia of inflammation, is a type II acute-phase protein. Blood **101**:2461–2463.

21. **Ludwiczek S, Aigner E, Theurl I, Weiss G, Marx JJ, Brock J.** 2003. Cytokine-

700 mediated regulation of iron transport in human monocytic cells. Blood **101**:4148–
701 54.
702 22. **Mpiga P, Ravaoarinoro M.** 2006. *Chlamydia trachomatis* persistence: An update.
703 Microbiol Res **161**:9-19.
704 23. **Theurl I, Theurl M, Seifert M, Mair S, Nairz M, Rumpold H, Zoller H,**
705 **Bellmann-Weiler R, Niederegger H, Talasz H, Weiss G.** 2008. Autocrine
706 formation of hepcidin induces iron retention in human monocytes. Blood
707 **111**:2392–9.
708 24. **Paradkar PN, De Domenico I, Durchfort N, Zohn I, Kaplan J, Ward DM.** 2008.
709 Iron depletion limits intracellular bacterial growth in macrophages. Blood **112**:866–
710 74.
711 25. **Nairz M, Haschka D, Demetz E, Weiss G.** 2014. Iron at the interface of immunity
712 and infection. Front Pharmacol **5**:152.
713 26. **Pokorzynski ND, Thompson CC, Carabeo RA.** 2017. Ironing out the
714 unconventional mechanisms of iron acquisition and gene regulation in *Chlamydia*.
715 Front Cell Infect Microbiol **7**:394.
716 27. **Hentze MW, Muckenthaler MU, Galy B, Camaschella C.** 2010. Two to tango:
717 regulation of Mammalian iron metabolism. Cell **142**:24–38.
718 28. **Vardhan H, Bhengraj AR, Jha R, Singh Mittal A.** 2009. *Chlamydia trachomatis*
719 alters iron-regulatory protein-1 binding capacity and modulates cellular iron
720 homeostasis in HeLa-229 cells. J Biomed Biotechnol 2009:342032. doi:
721 10.1155/2009/342032.
722 29. **Kim I, Yetley EA, Calvo MS.** 1993. Variations in iron-status measures during the

723 menstrual cycle. Am J Clin Nutr **58**:705–9.

724 30. **Kelver ME, Kaul A, Nowicki B, Findley WE, Hutchens TW, Nagamani M.** 1996.
725 Estrogen regulation of lactoferrin expression in human endometrium. Am J
726 Reprod Immunol **36**:243–7.

727 31. **Aisen P, Enns C, Wessling-Resnick M.** 2001. Chemistry and biology of
728 eukaryotic iron metabolism. Int J Biochem Cell Biol **33**:940–959.

729 32. **Skaar EP.** 2010. The battle for iron between bacterial pathogens and their
730 vertebrate hosts. PLoS Pathog 6:e1000949. doi: 10.1371/journal.ppat.1000949.

731 33. **Caza M, Kronstad JW.** 2013. Shared and distinct mechanisms of iron acquisition
732 by bacterial and fungal pathogens of humans. Front Cell Infect Microbiol **3**:80.

733 34. **Hood MI, Skaar EP.** 2012. Nutritional immunity: transition metals at the
734 pathogen–host interface. Nat Rev Microbiol **10**:525–537.

735 35. **Pan X, Tamilselvam B, Hansen EJ, Daefler S. 2010.** Modulation of iron
736 homeostasis in macrophages by bacterial intracellular pathogens. BMC Microbiol
737 **10**:64.

738 36. **Scidmore MA, Fischer ER, Hackstadt T.** 2003. Restricted fusion of *Chlamydia*
739 *trachomatis* vesicles with endocytic compartments during the initial stages of
740 infection. Infect Immun **71**:973–84.

741 37. **Ouellette SP, Carabeo RA.** 2010. A functional slow recycling pathway of
742 transferrin is required for growth of *Chlamydia*. Front Microbiol **1**:1–12.

743 38. **Boradia VM, Malhotra H, Thakkar JS, Tillu VA, Vuppala B, Patil P, Sheokand**
744 **N, Sharma P, Chauhan AS, Raje M, Raje CI.** 2014. *Mycobacterium tuberculosis*
745 acquires iron by cell-surface sequestration and internalization of human holo-

746 transferrin. Nat Commun **5**:4730.

747 39. **Raulston JE, Miller JD, Davis CH, Schell M, Baldwin A, Ferguson K, Lane H.**
748 2007. Identification of an iron-responsive protein that is antigenic in patients with
749 *Chlamydia trachomatis* genital infections. FEMS Immunol Med Microbiol **51**:569–
750 76.

751 40. **Miller JD, Sal MS, Schell M, Whittimore JD, Raulston JE.** 2009. *Chlamydia*
752 *trachomatis* YtgA is an iron-binding periplasmic protein induced by iron restriction.
753 Microbiology **155**:2884–94.

754 41. **Thompson CC, Nicod SS, Malcolm DS, Grieshaber SS, Carabeo RA.** 2012.
755 Cleavage of a putative metal permease in *Chlamydia trachomatis* yields an iron-
756 dependent transcriptional repressor. Proc Natl Acad Sci U S A **109**:10546–51.

757 42. **Thompson CC, Carabeo RA. 2011.** An optimal method of iron starvation of the
758 obligate intracellular pathogen, *Chlamydia trachomatis*. Front Microbiol **2**:20.

759 43. **LaRue RW, Dill BD, Giles DK, Whittimore JD, Raulston JE.** 2007. Chlamydial
760 Hsp60-2 is iron responsive in *Chlamydia trachomatis* serovar E-infected human
761 endometrial epithelial cells *in vitro*. Infect Immun **75**:2374–80.

762 44. **Dill BD, Dessus-Babus S, Raulston JE.** 2009. Identification of iron-responsive
763 proteins expressed by *Chlamydia trachomatis* reticulate bodies during intracellular
764 growth. Microbiology **155**:210–9.

765 45. **Timms P.** 2009. Differential transcriptional responses between the interferon-
766 gamma-induction and iron-limitation models of persistence for *Chlamydia*
767 *pneumoniae.* J Microbiol Immunol Infect **42**:27-37.

768 46. **Consortium U.** 2017. UniProt: the universal protein knowledgebase. Nucleic

Acids Res **45**:D158–D169.

47. **Szklarczyk D, Franceschini A, Wyder S, Forslund K, Heller D, Huerta-Cepas J, Simonovic M, Roth A, Santos A, Tsafou KP, Kuhn M, Bork P, Jensen LJ, von Mering C.** 2015. STRING v10: protein-protein interaction networks, integrated over the tree of life. Nucleic Acids Res **43**:D447–D452.

48. **Kanehisa M, Goto S, Sato Y, Furumichi M, Tanabe M.** 2012. KEGG for integration and interpretation of large-scale molecular data sets. Nucleic Acids Res **40**:D109-14.

49. **Fehlner-Gardiner C, Roshick C, Carlson JH, Hughes S, Belland RJ, Caldwell HD, McClarty G.** 2002. Molecular basis defining human *Chlamydia trachomatis* tissue tropism. A possible role for tryptophan synthase. J Biol Chem **277**:26893–903.

50. **Wood H, Fehlner-Gardner C, Berry J, Fischer E, Graham B, Hackstadt T, Roshick C, McClarty G.** 2003. Regulation of tryptophan synthase gene expression in *Chlamydia trachomatis*. Mol Microbiol **49**:1347–1359.

51. **Caldwell HD, Wood H, Crane D, Bailey R, Jones RB, Mabey D, Maclean I, Mohammed Z, Peeling R, Roshick C, Schachter J, Solomon AW, Stamm WE, Suchland RJ, Taylor L, West SK, Quinn TC, Belland RJ, McClarty G.** 2003. Polymorphisms in *Chlamydia trachomatis* tryptophan synthase genes differentiate between genital and ocular isolates. J Clin Invest **111**:1757–69.

52. **Karayiannis P, Hobson D.** 1981. Amino acid requirements of a *Chlamydia trachomatis* genital strain in McCoy cell cultures. J Clin Microbiol **13**:427–32.

53. **Al-Younes HM, Gussmann J, Braun PR, Brinkmann V, Meyer TF.** 2006.

Naturally occurring amino acids differentially influence the development of *Chlamydia trachomatis* and *Chlamydia* (*Chlamydophila*) *pneumoniae*. J Med Microbiol **55**:879–886.

54. **Braun PR, Al-Younes H, Gussmann J, Klein J, Schneider E, Meyer TF.** 2008. Competitive inhibition of amino acid uptake suppresses chlamydial growth: involvement of the chlamydial amino acid transporter BrnQ. J Bacteriol **190**:1822–1830.

55. **Kane CD, Vena RM, Ouellette SP, Byrne GI.** 1999. intracellular tryptophan pool sizes may account for differences in gamma interferon-mediated inhibition and persistence of chlamydial growth in polarized and nonpolarized cells. Infect Immun **67**:1666–1671.

56. **Leonhardt RM, Lee SJ, Kavathas PB, Cresswell P.** 2007. Severe tryptophan starvation blocks onset of conventional persistence and reduces reactivation of *Chlamydia trachomatis*. Infect Immun **75**:5105–5117.

57. **Mi H, Huang X, Muruganujan A, Tang H, Mills C, Kang D, Thomas PD.** 2017. PANTHER version 11: expanded annotation data from Gene Ontology and Reactome pathways, and data analysis tool enhancements. Nucleic Acids Res **45**:D183–D189.

58. **Caspi R, Billington R, Ferrer L, Foerster H, Fulcher CA, Keseler IM, Kothari A, Krummenacker M, Latendresse M, Mueller LA, Ong Q, Paley S, Subhraveti P, Weaver DS, Karp PD.** 2016. The MetaCyc database of metabolic pathways and enzymes and the BioCyc collection of pathway/genome databases. Nucleic Acids Res **44**:D471–D480.

59. **Liechti GW, Kuru E, Hall E, Kalinda A, Brun Y V., VanNieuwenhze M, Maurelli AT.** 2013. A new metabolic cell-wall labelling method reveals peptidoglycan in *Chlamydia trachomatis*. Nature **506**:507–510.

60. **Soupene E, Wang D, Kuypers FA.** 2015. Remodeling of host phosphatidylcholine by *Chlamydia* acyltransferase is regulated by acyl-CoA binding protein ACBD6 associated with lipid droplets. Microbiologyopen **4**:235.

61. **Al-Younes HM, Rudel T, Brinkmann V, Szczepek AJ, Meyer TF.** 2001. Low iron availability modulates the course of *Chlamydia pneumoniae* infection. Cell Microbiol **3**:427–437.

62. **Mäurer AP, Mehlitz A, Mollenkopf HJ, Meyer TF.** 2007. Gene expression profiles of *Chlamydophila pneumoniae* during the developmental cycle and iron depletion-mediated persistence. PLoS Pathog **3**:0752–0769.

63. **Mukhopadhyay S, Miller RD, Sullivan ED, Theodoropoulos C, Mathews SA, Timms P, Summersgill JT.** 2006. Protein expression profiles of *Chlamydia pneumoniae* in models of persistence versus those of heat shock stress response. Infect Immun **74**:3853–3863.

64. **Jain V, Kumar M, Chatterji D.** 2006. ppGpp: stringent response and survival. J Microbiol **44**:1–10.

65. **Potrykus K, Murphy H, Philippe N, Cashel M.** 2011. ppGpp is the major source of growth rate control in *E. coli.* Environ Microbiol **13**:563–575.

66. **Perederina A, Svetlov V, Vassylyeva MN, Tahirov TH, Yokoyama S, Artsimovitch I, Vassylyev DG.** 2004. regulation through the secondary channel—structural framework for ppGpp-DksA synergism during transcription.

838 Cell **118**:297–309.

839 67. **Cashel M.** 1969. The control of ribonucleic acid synthesis in *Escherichia coli.* IV.
840 Relevance of unusual phosphorylated compounds from amino acid-starved
841 stringent strains. J Biol Chem **244**:3133–41.

842 68. **Haseltine WA, Block R.** 1973. Synthesis of guanosine tetra- and
843 pentaphosphate requires the presence of a codon-specific, uncharged transfer
844 ribonucleic acid in the acceptor site of ribosomes. Proc Natl Acad Sci U S A
845 **70**:1564–8.

846 69. **Traxler MF, Summers SM, Nguyen H-T, Zacharia VM, Hightower GA, Smith**
847 **JT, Conway T.** 2008. The global, ppGpp-mediated stringent response to amino
848 acid starvation in *Escherichia coli.* Mol Microbiol **68**:1128–1148.

849 70. **Mittenhuber G.** 2001. Comparative genomics and evolution of genes encoding
850 bacterial (p)ppGpp synthetases/hydrolases (the Rel, RelA and SpoT proteins). J
851 Mol Microbiol Biotechnol **3**:585–600.

852 71. **Ouellette SP, Rueden KJ, Rucks EA.** 2016. tryptophan codon-dependent
853 transcription in *Chlamydia pneumoniae* during gamma interferon-mediated
854 tryptophan limitation. Infect Immun **84**:2703–2713.

855 72. **Lo C-C, Xie G, Bonner CA, Jensen RA.** 2012. The alternative translational
856 profile that underlies the immune-evasive state of persistence in Chlamydiaceae
857 exploits differential tryptophan contents of the protein repertoire. Microbiol Mol
858 Biol Rev **76**:405–443.

859 73. **Bonner CA, Byrne GI, Jensen RA. 2014.** *Chlamydia* exploit the mammalian
860 tryptophan-depletion defense strategy as a counter-defensive cue to trigger a

861 survival state of persistence. Front Cell Infect Microbiol **4**:17.

862 74. **Akers JC, Tan M.** 2006. Molecular mechanism of tryptophan-dependent
863 transcriptional regulation in *Chlamydia trachomatis*. J Bacteriol **188**:4236–4243.

864 75. **Carlson JH, Wood H, Roshick C, Caldwell HD, McClarty G.** 2006. *In vivo* and
865 *in vitro* studies of *Chlamydia trachomatis* TrpR:DNA interactions. Mol Microbiol
866 **59**:1678–91.

867 76. **Amirshahi A, Wan C, Beagley K, Latter J, Symonds I, Timms P.** 2011.
868 Modulation of the *Chlamydia trachomatis in vitro* transcriptome response by the
869 sex hormones estradiol and progesterone. BMC Microbiol **11**:150.

870 77. **Rosenkranz HS, Gutter B, Becker Y.** 1973. Studies on the developmental cycle
871 of *Chlamydia trachomatis*: selective inhibition by hydroxyurea. J Bacteriol
872 **115**:682–90.

873 78. **Dassama LMK, Boal AK, Krebs C, Rosenzweig AC, Bollinger JM**. 2012.
874 Evidence that the β subunit of *Chlamydia trachomatis* ribonucleotide reductase is
875 active with the manganese Ion of Its manganese(IV)/iron(III) cofactor in site 1. J
876 Am Chem Soc **134**:2520–2523.

877 79. **Odsbu I, Morigen S, Skarstad K, Beckwith J, Beckwith J.** 2009. A reduction in
878 ribonucleotide reductase activity slows down the chromosome replication fork but
879 does not change its localization. PLoS One 4:e7617. 10.3389/fmicb.2011.00020.

880

881

882

TABLES

Table 1. Summary of RNA-sequencing and mapping in this study.

Sample	Total reads	Mapped reads (%)	Average read length	Coverage	Unique reads (%)	Gene reads (%)	Intergenic reads (%)
6+3BPD_01	31,783,753	94042 (0.3)	111.7	10.0	55784 (59)	72,201 (77)	21,841 (23)
6+3BPD_02	25,001,608	102978 (0.4)	100.6	9.9	62238 (60)	80076 (78)	22902 (22)
6+3BPD_03	26,362,915	81,301 (0.3)	111.6	8.7	42734 (53)	64,148 (79)	17153 (21)
9h_01	26,391,673	76603 (0.3)	104.3	7.6	48,904 (64)	59,462 (78)	17,141 (22)
9h_02	18,899,700	126725 (0.7)	111.1	13.5	82938 (65)	101,114 (80)	25,611 (20)
9h_03	24,659,022	110,564 (0.5)	119.6	12.6	59,941 (54)	88,214 (80)	22,350 (20)
12h_01	11,406,647	1,183,621 (10)	133.7	151.0	1014565 (86)	972,501 (82)	211,120 (18)
12h_02	18,794,400	1,826,559 (10)	132	230.0	1,532,588 (84)	1,502,698 (82)	323,861 (18)
12h_03	6,105,409	674,170 (11)	92.7	59.7	599,579 (89)	541,378 (80)	132,792 (20)
12h_04	5,490,040	275,903 (5)	122.3	32.2	228,625 (83)	216,560 (78)	59,343 (22)
12h_05	5,238,854	164239 (3)	124.1	19.5	127329 (78)	130,139 (79)	34,046 (21)
12+3BPD_01	12,936,290	1,446,925 (11)	123.6	170.9	1,320,489 (91)	1,2241,509 (86)	205,416 (14)
12+3BPD_02	14,147,695	1054535 (7)	129.6	130.6	962069 (91)	902519 (86)	152,016 (14)
12+3BPD_03	8,479,156	791,034 (9)	97.8	73.9	685,947 (87)	644,706 (82)	146,328 (18)
12+3BPD_04	4,628,453	1,044,587 (23)	131.2	131.0	870,713 (83)	812,561 (78)	232,026 (22)
12+3BPD_05	4,817,344	536875 (11)	122	62.6	418,855 (78)	421,924 (79)	114,951 (21)
15h_01	29,595,055	5499663 (19)	129.8	682.2	5106298 (93)	4,947,981 (90)	551,682 (10)
15h_02	22,517,134	2,643,605 (12)	117.3	60.2	915,409 (35)	2,348,719 (89)	294886 (11)
15h_03	11,378,770	239,110 (2)	100.3	22.9	112,935 (47)	202,415 (85)	36,695 (15)
15h_04	3,758,844	115863 (3)	106.5	11.8	73,387 (63)	95,335 (82)	20,528 (18)
12+6BPD_01	12,105,447	1,723,006 (14)	117.9	194.1	1,419,066 (82)	1,421,098 (82)	301,908 (18)
12+6BPD_02	14,751,746	1,131,903 (8)	111.6	120.7	912,764 (81)	907,278 (80)	224,625 (20)
12+6BPD_03	13,949,255	2,024,141 (15)	96	185.7	1,812,201 (90)	1666346 (82)	357795 (18)
18h_01	18,794,400	1,826,559 (10)	109.2	190.6	1,532,588 (84)	1,502,698 (82)	323,861 (18)
18h_02	13,002,450	553,409 (4)	117.3	62.0	470,659 (85)	454,119 (82)	99,290 (18)
18h_03	10,676,991	1,589,307 (15)	91.9	139.6	1,441,562 (91)	1,287,668 (81)	301,639 (19)

Table 2. Differentially expressed genes after 3h BPD treatment during mid-cycle development.

Feature ID	Locus tag	Fold change	P-value	FDR P-value correction	Annotation	Functional category	UniProtKB ID
CTL0013	CTL0013	3.45	3.10E-04	0.02	hypothetical, YGGT family	Hypothetical	A0A0H3MB25
trpB	CTL0423	3.18	3.23E-07	2.86E-04	tryptophan synthase subunit B	Amino acid biosynthesis	A0A0H3MD30
glgA	CTL0167	2.95	1.24E-04	8.99E-03	glycogen synthase	Energy Metabolism	B0B925
murB	CTL0203	2.52	6.41E-03	0.11	UDP-N-acetylenolpyruvoylglucosamine reduc	Other	B0B960
CTL0525	CTL0525	2.38	4.53E-05	5.02E-03	TPR-containing domain	Hypothetical	A0A0H3MKX6
recA	CTL0018	2.21	1.98E-03	0.06	recombinase A	DNA replication and repair	B0B8M5
CTL0339	CTL0339	2.2	2.29E-03	0.06	phosphatidylcholine-hydrolyzing phospholipas	Other	A0A0H3MCY1
aroL	CTL0621	2.13	6.56E-03	0.11	shikimate kinase 2	Amino acid biosynthesis	A0A0H3MDG7
hemE	CTL0116	2.09	1.68E-03	0.05	uroporphyrinogen decarboxylase	Cofactor biosynthesis	B0B8X3
CTL0408	CTL0408	2.08	1.36E-05	1.87E-03	MIR, MAC/perforin domain-containing protein	Other	A0A0H3MGT6
nrdA	CTL0199	2	1.48E-05	1.87E-03	Ribonucleoside-diphosphate reductase	DNA replication and repair	A0A0H3MCP2
mqnD	CTL0514	2	2.45E-03	0.06	1,4-dihydroxy-6-naphtoate synthase	Cofactor biosynthesis	A0A0H3MC13
CTL0704	CTL0704	1.99	0.01	0.16	hypothetical	Hypothetical	A0A0H3MCH5
trpA	CTL0424	1.94	4.15E-03	8.00E-02	tryptophan synthase subunit A	Amino acid biosynthesis	A0A0H3MKP4
CTL0255	CTL0255	1.93	4.37E-03	0.09	hypothetical	Hypothetical	A0A0H3MGJ2
pepF	CTL0367	1.9	6.17E-04	0.03	endopeptidase F	Protein processing and folding	A0A0H3MKK2
rnc	CTL0549	1.89	0.01	0.14	ribonuclease III	Transcriptional regulation	B0B7L3
CTL0823	CTL0823	1.88	7.21E-04	0.03	hypothetical	Hypothetical	A0A0H3MLF6
CTL0301	CTL0301	1.81	1.32E-04	8.99E-03	probable cytosol aminopeptidase pepA	Protein processing and folding	B0B9F3
CTL0884	CTL0884	1.81	7.04E-03	0.11	hypothetical	Hypothetical	A0A0H3MCL0
CTL0885	CTL0885	1.77	3.48E-03	0.08	hypothetical effector	Type III Secretion	A0A0H3MHM9
lpdA	CTL0820	1.76	3.80E-03	0.08	dihydrolipoyl dehydrogenase	Energy Metabolism	A0A0H3MHJ2
CTL0096	CTL0096	1.72	1.98E-04	0.01	putative cation transporting ATPase	Nutrient transport	A0A0H3MCG9
gp6D	CTL0846	1.72	2.77E-03	0.07	virulence plasmid pGP6-D related protein	Hypothetical	A0A0H3MLH1
dnaQ	CTL0513	1.69	0.01	0.15	DNA polymerase III subunit epsilon	DNA replication and repair	A0A0H3MKW6
CTL0512	CTL0512	1.68	4.52E-03	0.09	mcsc, secretion chaperone	Type III Secretion	A0A0H3MDA7
CTL0847	CTL0847	1.63	6.69E-03	0.11	hypothetical	Hypothetical	A0A0H3MCR9
oppA3	CTL0450	1.61	9.20E-03	0.13	oligopeptide transporter	Nutrient transport	A0A0H3MKR3
CTL0102	CTL0102	1.6	7.09E-03	0.11	putative exported protein	Hypothetical	A0A0H3MG91
lipA	CTL0821	1.59	8.90E-03	0.13	lipioic acid synthase	Other	B0B8D2
pheT	CTL0736	1.59	0.01	0.17	phenylalanine--tRNA ligase beta subunit	Translation	A0A0H3MHF2
cysS	CTL0151	1.56	2.47E-03	0.06	cysteinyl-tRNA synthetase	Translation	A0A0H3MGC2
CTL0055	CTL0055	1.51	7.04E-03	0.11	hypothetical	Hypothetical	A0A0H3MAN0
pal	CTL0863	1.51	7.29E-03	0.11	peptidogycan-associated lipoprotein	Other	A0A0H3MDU9
thrS	CTL0844	1.48	6.31E-03	0.11	threonine-tRNA ligase	Translation	B0B8F5
CTL0476	CTL0476	1.48	0.01	0.15	candidate inclusion membrane protein	Hypothetical	A0A0H3MKT3
CTL0043	CTL0043	1.46	0.01	0.15	type III secretion structural protein	Type III Secretion	A0A0H3MG59
glmS	CTL0188	1.46	0.01	0.16	Glutamine--fructose-6-phosphate aminotransf	Energy Metabolism	A0A0H3MCN0
CTL0684	CTL0684	1.45	8.29E-03	0.12	hypothetical	Hypothetical	A0A0H3MCF9
nusA	CTL0352	-1.48	4.90E-03	0.09	transcription termination factor	Transcriptional regulation	A0A0H3MGQ1
prfA	CTL0278	-1.56	9.49E-03	0.13	Peptide chain release factor RF1	Translation	B0B9D0
rplW	CTL0788	-1.58	5.43E-04	0.02	ribosomal subunit	Translation	B0B8A0
CTL0326	CTL0326	-1.62	6.61E-03	0.11	ytgD, ABC transport protein, membrane perm	Nutrient transport	A0A0H3MGN6
trpF	CTL0581	-1.67	2.26E-03	0.06	N-(5'-phosphoribosyl)anthranilate isomerase	Cofactor biosynthesis	B0B7P4
folX	CTL0878	-1.68	7.23E-03	0.11	Dihydroneopterin triphosphate 2'-epimerase	Cofactor biosynthesis	A0A0H3MCK6
pgsA_2	CTL0757	-1.71	1.74E-03	0.05	CDP-diacylglycerol--glycerol-3-phosphate 3-p	Other	A0A0H3MHG9
sodM	CTL0546	-1.74	1.46E-03	0.05	superoxide dismutase	Redox homeostasis	A0A0H3MKY6
CTL0138	CTL0138	-1.74	4.48E-03	0.09	ribosomal silencing factor RsfS	Translation	A0A0H3MAQ8
CTL0061	CTL0061	-1.75	2.26E-04	0.01	inorganic phosphate transporter	Nutrient transport	A0A0H3MG71
CTL0486	CTL0486	-1.77	3.48E-03	0.08	putative membrane transport protein	Nutrient transport	A0A0H3MBY7
gltT	CTL0658	-1.85	3.07E-03	0.07	sodium:dicarboxylate symport protein	Nutrient transport	A0A0H3MCC1
smpB	CTL0332	-1.88	0.01	0.14	SsrA-binding protein	Translation	A0A0H3MBC6
aroA	CTL0620	-1.91	1.85E-04	0.01	3-phosphoshikimate 1-carboxyvinyltransferas	Energy Metabolism	B0B7T5
CTL0132	CTL0132	-1.92	3.03E-03	0.07	UPF0109-containing putative RNA-binding pr	Translation	A0A0H3MAQ7
CTL0548	CTL0548	-1.98	1.14E-04	8.99E-03	dcrA, putative non-heme Fe(II) 2-oxoglutarate	Hypothetical	A0A0H3MBY2
secG	CTL0606	-2.01	0.01	0.14	Protein-export membrane protein SecG	Protein processing and folding	A0A0H3MH61
rpsK	CTL0770	-2.07	1.59E-06	4.79E-04	ribosomal subunit	Translation	B0B882
rplT	CTL0207	-2.07	1.62E-06	4.79E-04	ribosomal subunit	Translation	B0B964
rplN	CTL0780	-2.08	3.98E-03	0.08	ribosomal subunit	Translation	B0B892
CTL0720	CTL0720	-2.12	5.09E-03	0.09	SWIB-domain containing protein	Hypothetical	A0A0H3MC95
gcsH	CTL0534	-2.14	9.08E-04	0.03	glycine cleavage system H protein	Amino acid biosynthesis	B0B7J8
CTL0680	CTL0680	-2.14	1.59E-03	0.05	putative rRNA processing peptide	Translation	A0A0H3MHB1
rpmI	CTL0206	-2.14	1.75E-03	0.05	ribosomal subunit	Translation	A0A0H3MCP7
fer	CTL0315	-2.26	6.48E-05	6.38E-03	ferredoxin	Redox homeostasis	A0A0H3MCW5
CTL0552	CTL0552	-2.27	1.09E-03	0.04	TPR-containing domain	Hypothetical	pseudogene
CTL0222	CTL0222	-2.27	6.58E-03	0.11	hypothetical	Hypothetical	A0A0H3MK96
infA2	CTL0575	-2.29	6.70E-06	1.19E-03	Translation initiation factor IF-1	Translation	A0A0H3MDD9
rpsT	CTL0881	-2.38	1.13E-04	8.99E-03	ribosomal subunit	Translation	B0B8J2
CTL0335	CTL0335	-2.43	0.01	0.17	Putative integral membrane protein	Hypothetical	A0A0H3MCX6
ltuA	CTL0631	-2.68	3.38E-03	0.08	Late transcription unit A protein	Hypothetical	A0A0H3MH76
rpsO	CTL0215	-2.72	4.14E-04	0.02	ribosomal subunit	Translation	B0B972
ndk	CTL0762	-2.76	7.97E-04	0.03	nucleoside diphosphate kinase	DNA replication and repair	B0B874
L2bCS78408_RS04755	L2bCS7840	-2.99	0.01	0.17	Virulence plasmid integrase pGP8-D	DNA replication and repair	B0BCM4
dut	CTL0544	-3.02	6.06E-06	1.19E-03	deoxyuridine 5'-triphosphate nucleotidohydrol	DNA replication and repair	B0B7K8
rpmJ	CTL0154	-3.03	3.18E-04	0.02	ribosomal subunit	Translation	B0B912
CTL0021	CTL0021	-3.16	0.01	0.17	hypothetical	Hypothetical	A0A0H3MG42

This data was exported from CLC Genomics Workbench 9.5.3. rRNAs, tRNAs, and Features (genes) with less than 10 reads in all samples were eliminated from the dataset prior to normalization and EDGE analysis, and only includes genes that were differentially expressed with a significance p-value ≤ 0.01.

885

Table 3. Differentially expressed genes after 6h BPD treatment during mid-cycle development.

Feature ID	Locus Tag	P-value	Fold change	FDR p-value correction	Annotation	Functional category	UniProtKB ID
trpB	CTL0423	2.61E-07	3.5	2.32E-04	tryptophan synthase subunit B	Amino acid biosynthesis	A0A0H3MD30
trpA	CTL0424	9.26E-06	3.21	2.73E-03	tryptophan synthase subunit A	Amino acid biosynthesis	A0A0H3MKP4
nrdA	CTL0199	3.50E-06	2.39	1.55E-03	ribonucleoside-diphosphate reductase	DNA replication and repair	A0A0H3MCP2
CTL0071	CTL0071	6.73E-03	1.73	0.55	hypothetical	Hypothetical	A0A0H3MCG5
nrdB	CTL0200	9.34E-03	1.63	0.69	ribonucleoside-diphosphate reductase	DNA replication and repair	A0A0H3MK81
CTL0619	CTL0619	1.68E-03	-1.83	0.21	hypothetical integral membrane protein	Hypothetical	A0A0H3MH71
copD	CTL0842	3.17E-03	-2.13	0.31	type III secretion system protein	Type III Secretion	A0A0H3MHK7
scc2	CTL0839	1.37E-03	-2.18	0.2	type III secretion system chaperone	Type III Secretion	A0A0H3MLG7
tsp	CTL0700	1.28E-03	-2.34	0.2	tail-specific protease	Protein processing and folding	A0A0H3MDM0
CTL0185	CTL0185	6.85E-03	-2.76	0.55	hypothetical membrane protein	Hypothetical	A0A0H3MAV2
copB	CTL0841	6.79E-05	-2.81	0.02	type III secretion system membrane protein	Type III Secretion	A0A0H3MCF0
CTL0840	CTL0840	2.15E-03	-2.97	0.24	hypothetical	Hypothetical	A0A0H3MCQ4

This data was exported from CLC Genomics Workbench 9.5.3. rRNAs, tRNAs, and Features (genes) with less than 10 reads in all samples were eliminated from the dataset prior to normalization and EDGE analysis. This data only includes genes that were differentially expressed with a significance p-value ≤ 0.01.

Table 4. Differentially expressed genes after 3h BPD treatment during early-cycle development.

Feature ID	Locus Tag	Fold change	P-value	FDR P-value correction	Annotation	Functional category	UniProtKB ID
CTL0149	CTL0149	6.71	3.71E-03	0.09	protein disulfide isomerase	Redox homeostasis	A0A0H3MAT1
CTL0184	CTL0184	3.4	4.44E-05	0.00493	hypothetical inclusion membrane protein	Hypothetical	A0A0H3MBD4
trpA	CTL0424	3.12	3.27E-04	0.02	tryptophan synthase subunit A	Amino acid biosynthesis	A0A0H3MKP4
CTL0388	CTL0388	2.93	3.02E-03	0.08	hypothetical methyltransferase	Hypothetical	A0A0H3MKL6
CTL0111	CTL0111	2.89	0.000877	0.04	rRNA methyltransferase TrmA	Translation	A0A0H3MAQ4
hemN_1	CTL0115	2.47	1.00E-02	0.19	coproporphyrinogen-III oxidase	Cofactor biosynthesis	A0A0H3MJY5
mip	CTL0803	2.37	3.97E-04	0.02	peptidyl-prolyl cis-trans isomerase	Protein processing and folding	A0A0H3MDR1
trpB	CTL0423	2.28	2.55E-03	0.08	tryptophan synthase subunit B	Amino acid biosynthesis	A0A0H3MD30
lpxB	CTL0668	2.28	0.00923	0.16	lipid-A-disaccharide synthase	Other	A0A0H3MDJ6
nrdB	CTL0200	2.12	1.57E-06	4.61E-04	ribonucleoside-diphosphate reductase subunit B	DNA replication and repair	A0A0H3MK81
nrdA	CTL0199	2.09	4.10E-12	3.65E-09	ribonucleoside-diphosphate reductase subunit A	DNA replication and repair	A0A0H3MCP2
CTL0874	CTL0874	2.04	2.07E-06	0.000461	CADD,PABA synthase	Cofactor biosynthesis	A0A0H3MHM3
CTL0360	CTL0360	2.04	8.59E-03	0.15	hypothetical	Hypothetical	A0A0H3MKJ7
mutS	CTL0160	1.95	6.41E-06	1.08E-03	DNA mismatch repair protein	DNA replication and repair	B0B918
dnaQ	CTL0513	1.88	2.83E-03	0.08	DNA polymerase III subunit epsilon	DNA replication and repair	A0A0H3MKW6
CTL0164	CTL0164	1.86	1.20E-03	5.00E-02	hypothetical exported protein	Hypothetical	A0A0H3MBC3
CTL0791	CTL0791	1.82	1.78E-07	7.92E-05	hypothetical membrane protein	Hypothetical	A0A0H3MCL8
trpS	CTL0848	1.81	1.46E-03	0.05	tryptophan-tRNA ligase	Translation	A0A0H3MCF4
aspC_1	CTL0005	1.77	1.92E-05	0.00244	aminotransferase	Amino acid biosynthesis	A0A0H3MG09
eno	CTL0850	1.75	2.51E-03	0.08	enolase	Energy Metabolism	B0B8G1
CTL0408	CTL0408	1.73	3.50E-04	2.00E-02	MIR, MAC/perforin domain-containing protein	Other	A0A0H3MGT6
recA	CTL0018	1.72	1.49E-03	0.05	recombinase A	DNA replication and repair	B0B8M5
sodM	CTL0546	1.65	7.17E-03	0.14	superoxide dismutase	Redox homeostasis	A0A0H3MKY6
brnQ	CTL0817	1.62	3.60E-04	2.00E-02	branched chain amino acid transporter	Nutrient transport	A0A0H3MLF2
greA	CTL0004	1.59	2.63E-04	0.02	transcription elongation factor	Transcriptional regulation	A0A0H3MAD9
CTL0102	CTL0102	1.58	4.63E-03	0.11	hypothetical exported protein	Hypothetical	A0A0H3MG91
ahpC	CTL0866	1.52	2.54E-03	8.00E-02	thio-specific antioxidant peroxidase	Redox homeostasis	A0A0H3MCJ5
thrS	CTL0844	1.52	0.00501	0.11	threonine-tRNA ligase	Translation	B0B8F5
aspS	CTL0804	1.52	6.89E-03	0.14	aspartate--tRNA ligase	Translation	B0B8B6
rpoD	CTL0879	1.51	1.00E-02	0.18	RNA polymerase sigma factor RpoD	Transcriptional regulation	A0A0H3MHM6
glyA	CTL0691	1.47	0.00242	0.08	serine hydroxymethyltransferase	Amino acid biosynthesis	B0B804
sctJ	CTL0822	1.43	7.93E-03	0.14	type III secretion protein	Type III Secretion	A0A0H3MDS0
rpoC	CTL0566	-1.28	7.87E-03	0.14	DNA-directed RNA polymerase subunit beta'	Transcriptional regulation	B0B7N0
L2bCS7840	L2bCS7840	-1.36	4.91E-03	0.11	virulence plasmid integrase pGP8-D	DNA replication and repair	B0BCM4
rplW	CTL0788	-1.41	0.0035	0.09	ribosomal subunit	Translation	B0B8A0
prfA	CTL0278	-1.44	5.80E-03	1.20E-01	peptide chain release factor RF1	Translation	B0B9D0
rplC	CTL0790	-1.52	4.30E-04	0.02	ribosomal subunit	Translation	B0B8A2
CTL0061	CTL0061	-1.52	2.95E-03	0.08	inorganic phosphate transporter PHO4	Nutrient transport	A0A0H3MG71
CTL0659	CTL0659	-1.57	9.75E-04	0.05	tetraacyldisaccharide 4'-kinase lpxK	Other	A0A0H3MC42
CTL0473	CTL0473	-1.57	1.22E-03	0.05	hypothetical exported protein	Hypothetical	A0A0H3MBQ9
incD	CTL0370	-1.59	3.33E-03	0.09	inclusion membrane protein D	Other	B0B9M3
plsX	CTL0182	-1.59	1.00E-02	0.19	phosphate acyltransferase	Other	B0B939
CTL0613	CTL0613	-1.6	1.34E-03	0.05	hypothetical inner membrane protein	Hypothetical	A0A0H3MC14
pmpA	CTL0669	-1.63	0.00534	0.11	probable outer membrane protein PmpA	Other	A0A0H3ML49
CTL0548	CTL0548	-1.66	1.01E-03	0.05	hypothtetical non-heme Fe(II) 2-oxoglutarate	Hypothetical	A0A0H3MBY2
CTL0541	CTL0541	-1.67	1.00E-02	0.22	hypothetical membrane protein	Hypothetical	A0A0H3MC35
sucB_2	CTL0311	-1.7	7.85E-03	1.40E-01	dihydrolipoyllysine-residue succinyltransferase	Energy Metabolism	A0A0H3ML42
amn	CTL0120	-1.71	4.71E-03	0.11	AMP nucleosidase	DNA replication and repair	A0A0H3MGA3
mrsA	CTL0547	-1.77	1.00E-02	0.19	phosphoglucomutase	Other	A0A0H3MC40
ftsY	CTL0192	-1.82	4.26E-04	0.02	signal recognition particle receptor	Translation	A0A0H3MGE5
CTL0609	CTL0609	-1.85	7.29E-06	0.00108	hypothetical exported protein	Hypothetical	A0A0H3MDF7
dnaX_1	CTL0439	-1.92	5.15E-03	1.10E-01	DNA polymerase III subunit gamma/tau	DNA replication and repair	A0A0H3MBM8
CTL0314	CTL0314	-2.04	2.67E-04	0.02	hypothetical membrane protein	Hypothetical	A0A0H3MGM7
CTL0430	CTL0430	-3.85	5.46E-05	0.00539	hypothetical integral membrane protein	Hypothetical	A0A0H3MBV0
CTL0063	CTL0063	-3.89	2.61E-03	0.08	hyptothetical	Hypothetical	A0A0H3MCG4

This data was exported from CLC Genomics Workbench 9.5.3. rRNAs, tRNAs, and Features (genes) with less than 10 reads in all samples were eliminated from the dataset prior to normalization and EDGE analysis. This data only includes genes that were differentially expressed with a significance p-value ≤ 0.01.

Table 5: Translation factors differentially expressed during mid-cycle iron-starvation.

Gene	Direction of expression change	Locus Tag	Protein ID	Annotation	Interacting component	Result of interaction	Change in gene expression at t6+3 hr BPD
tRNA processing							
rnpA_1	decrease	CTL0153	RnP1	Ribonuclease P protein component	tRNA	cleaves 5' end of pre-tRNA	
rnpA_2	decrease	CTL0153A	RnP2	Ribonuclease P protein component	tRNA	cleaves 5' end of pre-tRNA	
tRNA Biogenesis							
cysS	increase	CTL0151	CysS	Cysteine-tRNA ligase	tRNA(Cys)	Charges tRNA with Cysteine	
pheT	increase	CTL0736	PheT	Phenylalanine-tRNA ligase beta subunit	tRNA(Phe)	Charges tRNA with Phenylalanine	
glyQ	increase	CTL0165	glyQ	Glycine-tRNA ligase alpha subunit	tRNA(Gly)	Charges tRNA with Glycine	
aspS	increase	CTL0804	AspS	Aspartate-tRNA ligase	tRNA(Asp)	Charges tRNA with Aspartate	increase
thrS	increase	CTL0844	ThrS	Threonine-tRNA ligase	tRNA(Thr)	Charges tRNA with Threonine	increase
truA	increase	CTL0723	TruA	tRNA pseudouridine synthase A	tRNA-anticodon loop	Converts uridines at 38, 39, 40 to pseudouridine	
miaA	increase	CTL0135	MiaA	tRNA dimethylallyltransferase	tRNA-anticodon loop	Converts adenine (37) to N6-(dimethylallyl)adenosine	
rRNA processing							
rnc	increase	CTL0549	Rnc	Rnase III	30s transcript	Cleaves 30s precursor transcript to 16S and 23S	increase
Subunit Assembly							
rpsO	decrease	CTL0215	S15	ribosomal protein	16s rRNA	Assembly of 30s subunit	
rpsT	decrease	CTL0881	S20	ribosomal protein	16s rRNA	Assembly of 30s subunit	
rpsK	decrease	CTL0770	S11	ribosomal protein	30s subunit	Forms Shine-Delgarno cleft	
rplT	decrease	CTL0207	L20	ribosomal protein	23s rRNA	Assembly of 50s subunit	
rplN	decrease	CTL0780	L14	ribosomal protein	23s rRNA	Forms bridge between 30s and 50s	
rplW	decrease	CTL0788	L23	ribosomal protein	23s rRNA	Forms docking site for trigger rf factor	decrease
Initiation							
infA2	decrease	CTL0575	IF-1	initiation factor	30S-RpsA	Recruited to 30S by RpsA	
	decrease		IF-1	initiation factor	IF-3	IF-1 and IF-3 recruit IF-2 to 30s, IF-2 recruits mRNA and tRNA	
rplN	decrease	CTL0780	L14	ribosomal protein	23s rRNA	Forms bridge between 30s and 50s	decrease
rsfS	decrease	CTL0138	RsfS	ribosomal silencing factor	RplN	Inhibits 70s assembly	
rplL	decrease	CTL0568	L7/L12	ribosomal protein	GTPases	Binds GTPases required for IF-3 recruitment	
Elongation							
rplL	decrease	CTL0568	L7/L12	ribosomal protein	GTPases	Binds GTPases required for EF-Tu and EF-G recruitment	
Termination							
prfA	decrease	CTL0278	RF-1	ribosome release factor		Increases termination at UAA and UAG stop codons	decrease
rplL	decrease	CTL0568	L7/L12	ribosomal protein	GTPases	GTPase activity required for RF-3 recruitment	
Recycling							
rrf	decrease	CTL0046	RrF	ribosome recycling factor		Causes disassembly of stalled ribosomes	
CTL0634	increase	CTL0634	HflX	GTPase HflX	50s subunit	Binds to E-site of 70s, disassembles ribosome	
Nascent Peptide Folding/Targeting							
ftsY	decrease	CTL0192	PtsY	Signal recognition particle receptor	SRP-RNC	Targets nascent membrane proteins to sec translocase	
secG	decrease	CTL0606	SecG	Protein-export membrane protein	SecY	Forms SecYEG translocation channel	
smpB	decrease	CTL0332	SmpB	SsrA-binding protein	tmRNA	Guides tmRNA into tRNA A site, rescuing stalled ribosomes and tagging nascent peptides for degradation	
Unknown Function							
rpmE	decrease	CTL0277	L31	ribosomal protein	23s rRNA	Unknown	
rplQ	decrease	CTL0768	L15	ribosomal protein	23s rRNA	Unknown	
rplY	decrease	CTL0168	L25	ribosomal protein	5s rRNA	Binds to 5s in central protuberance	

These genes were shown to be differentially regulated by EDGER analysis in CLC Genomics Workbench with p-value ≤ 0.05 during mid-cycle iron-starvation (12+3 BPD vs t5 h). Annotations and functions were retrieved from UniProt and BioCyc databases.

898 FIGURES

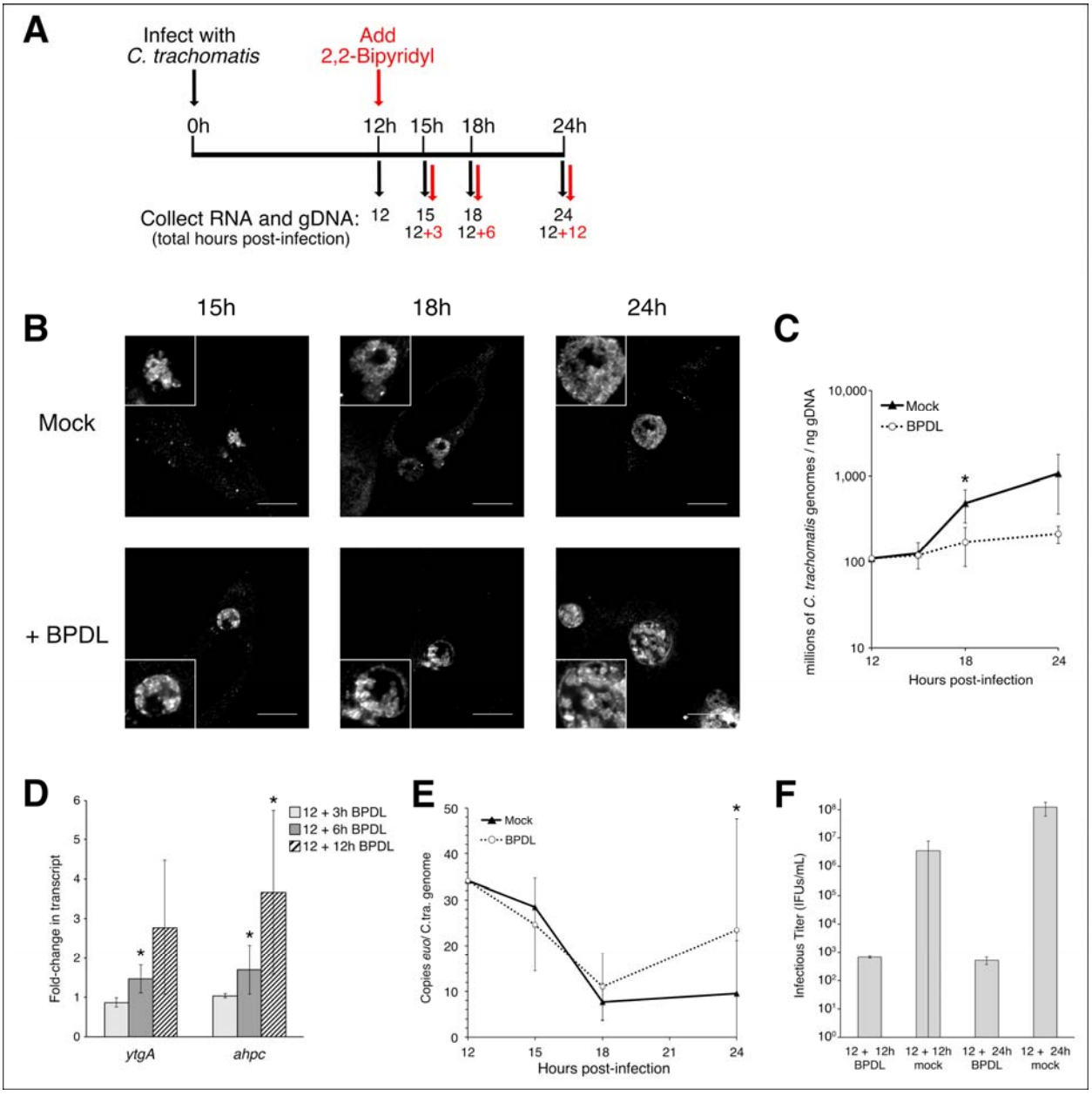

899

900 **Figure 1. Optimization of 2,2-Bipyrdyl (BPDL) treatment to induce iron-**
901 **responsiveness in the absence of persistence.** Timeline of BPDL-treatment A)
902 starting at 12h p.i., BPDL was supplemented to culture media for 3, 6, or 12h. Mock-
903 treated and BPDL-treated samples were tested for changes to B) morphology by
904 confocal microscopy, C) growth by qPCR, D) iron-responsive transcription (*ytgA, ahpC*)

905 D), and transcription of the developmental marker, *euo*, by RT-qPCR. Significant
906 changes with a p-value $\leq$ 0.05 in a one-tailed Student's t-test are indicated with an
907 asterisk, and are based on 3 biological replicates for the growth curve and 4 biological
908 replicates for RT-qPCR.

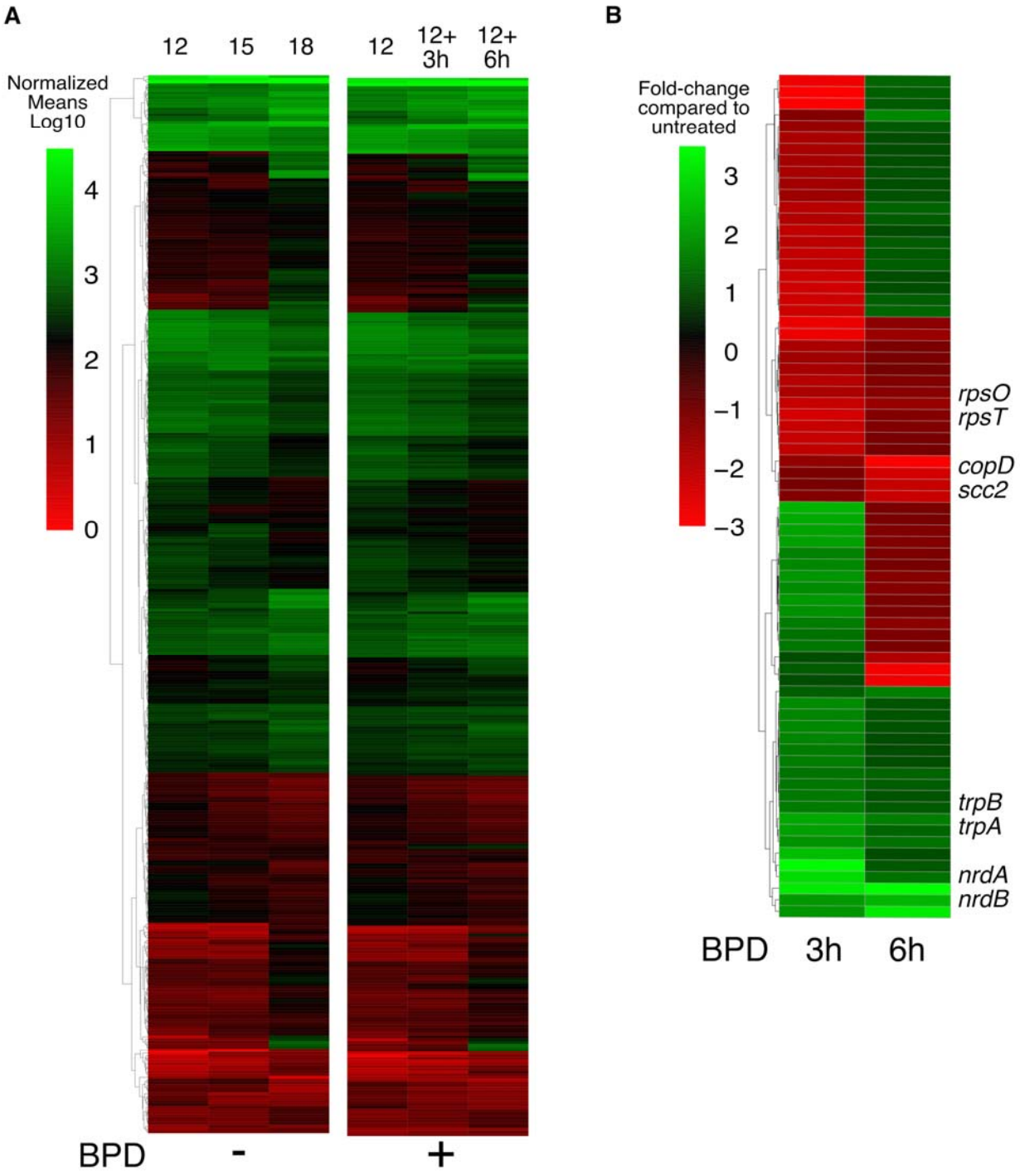

Figure 2. Global and differential gene expression of the mid-cycle response to iron-starvation. The global response of *C. trachomatis* to iron starvation was detected by RNA-sequencing and reads were aligned to the genome and plasmid. A) The untreated expression profile is displayed for all genes that change significantly (p-value

914 ≤ 0.01) during mid-cycle development as a heatmap of log10 transformed normalized
915 expression means (left). Expression across the same genes are displayed for BPDL-
916 treated samples (right). The highest and lowest expression values are displayed in
917 green and red, respectively. B) Genes that are significantly changed in response to iron-
918 starvation, with a p-value ≤ 0.01, are displayed as a heatmap of fold-changes of BPDL-
919 treated compared to mock-treated equivalent samples. The most highly up-regulated
920 and down-regulated transcripts are displayed in green and red, respectively.
921

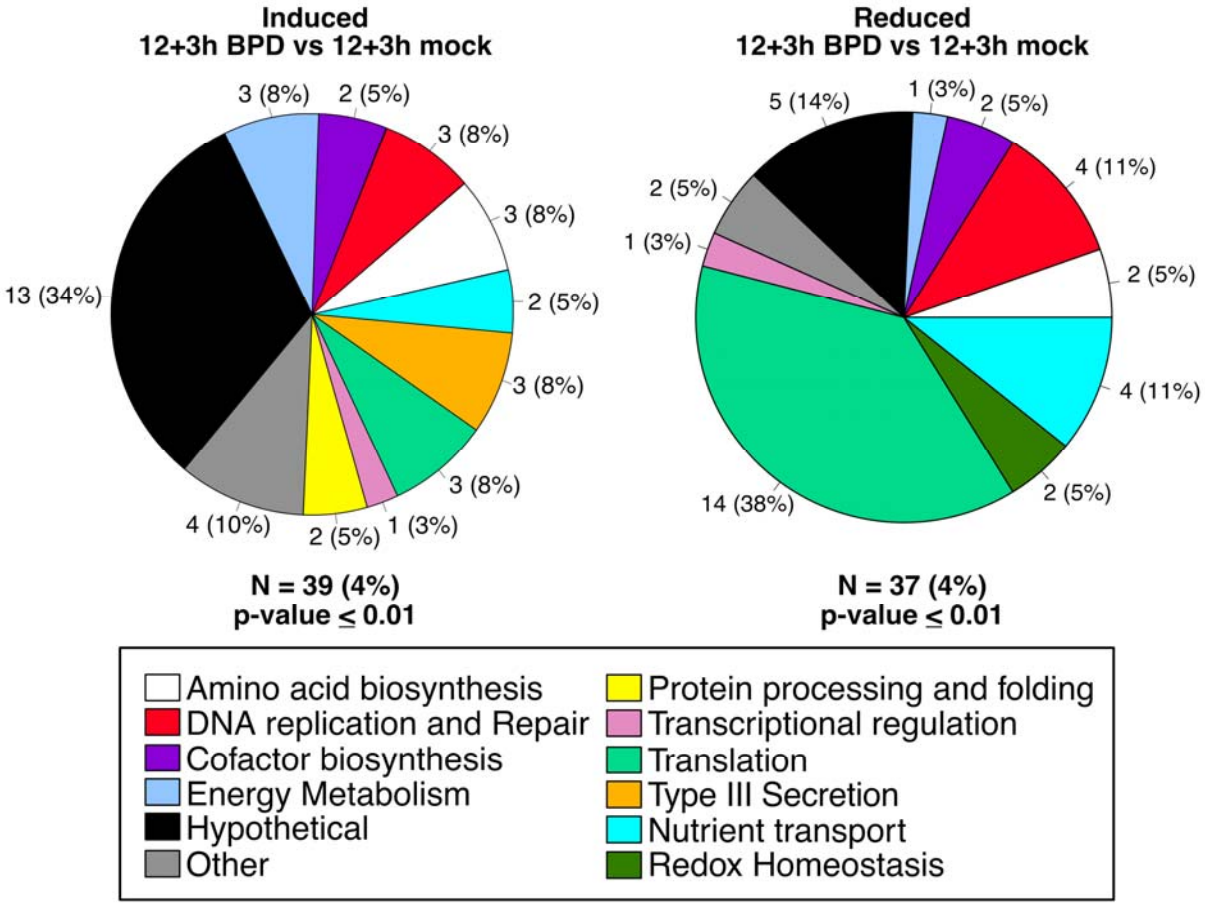

Figure 3. Functional categorization of mid-cycle response to iron-starvation. Transcripts that were significantly up-regulated (left) or down-regulated (right) after 3h BPDL treatment, starting at 12h p.i., are organized in pie charts by their functional categories. Adjacent to each pie slice is the number of genes in that category, and in parenthesis is the percentage of differentially expressed genes in the category. N=number of differentially expressed genes, and the percentage of the total genome that is represented.

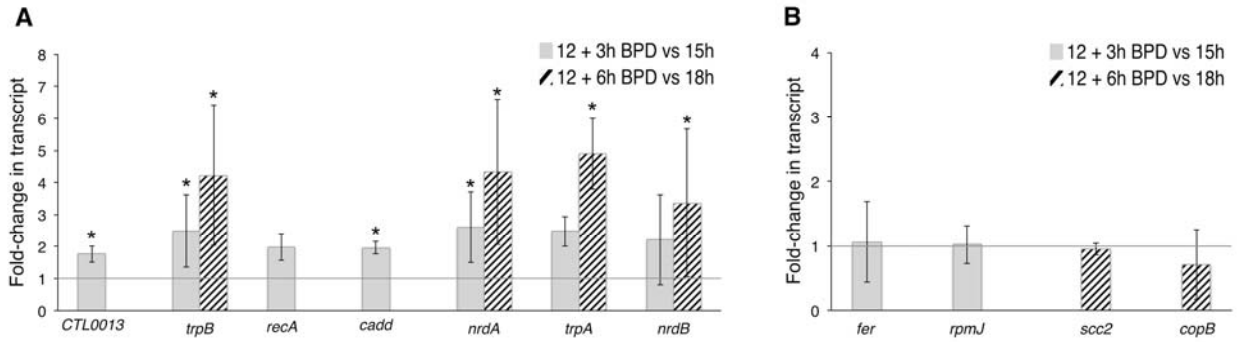

Figure 4. Confirmation of the mid-cycle response to iron starvation by RT-qPCR. Differentially expressed transcripts detected by RNA-sequencing were confirmed by RT-qPCR. A) Up-regulated or B) down-regulated transcription is indicated as fold-changes in transcripts after 3h BPD-treatment (solid gray bar) or 6h BPDL-treatment (striped bar) compared to mock-treated samples at equivalent timepoints post-infection. An asterisk indicates that the fold-change is significantly changed, with a p-value $\leq$ 0.05. Statistical analysis was done with a one-tailed Student's t-test, based on at least 3 biological replicates.

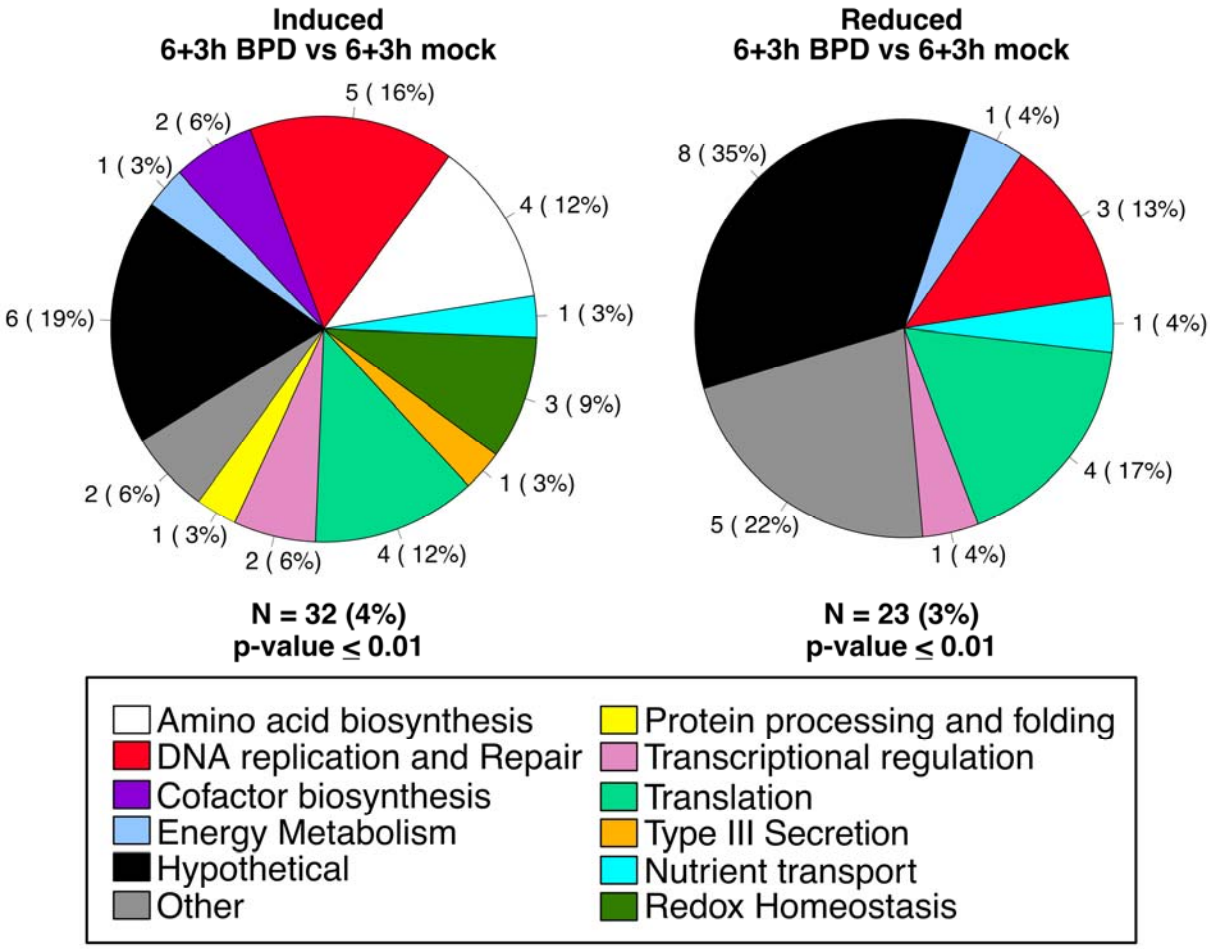

Figure 5. Functional categorization of the early-cycle response to iron-starvation. Transcripts that were significantly up-regulated (left) or down-regulated (right) after 3h of BPDL treatment, starting at 6h p.i., are organized in pie charts by their functional categories. Adjacent to each pie slice is the number of genes in that category, and in parenthesis is the percentage of differentially expressed genes in the category that make up the pie. N=number of differentially expressed genes, and the percentage of the total genome represented.

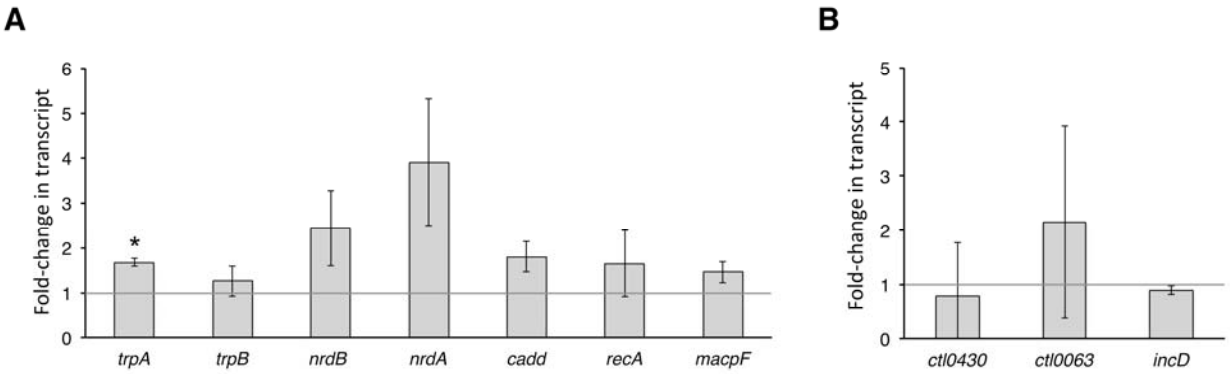

Figure 6. Confirmation of the early-cycle response to iron starvation by RT-qPCR. Transcripts that were significantly changed by RNA-sequencing, in response to iron-starvation starting at 6h p.i., were confirmed by RT-qPCR. A) Up-regulated or B) down-regulated transcription is indicated as fold-changes in transcripts after 3h BPDL-treatment in comparison to mock-treated at equivalent timepoints post-infection (solid gray bar). An asterisk indicates that the fold-change is significantly changed, with a p-value $\leq$ 0.05. Statistical analysis was done with a one-tailed Student's t-test, based on two biological replicates.

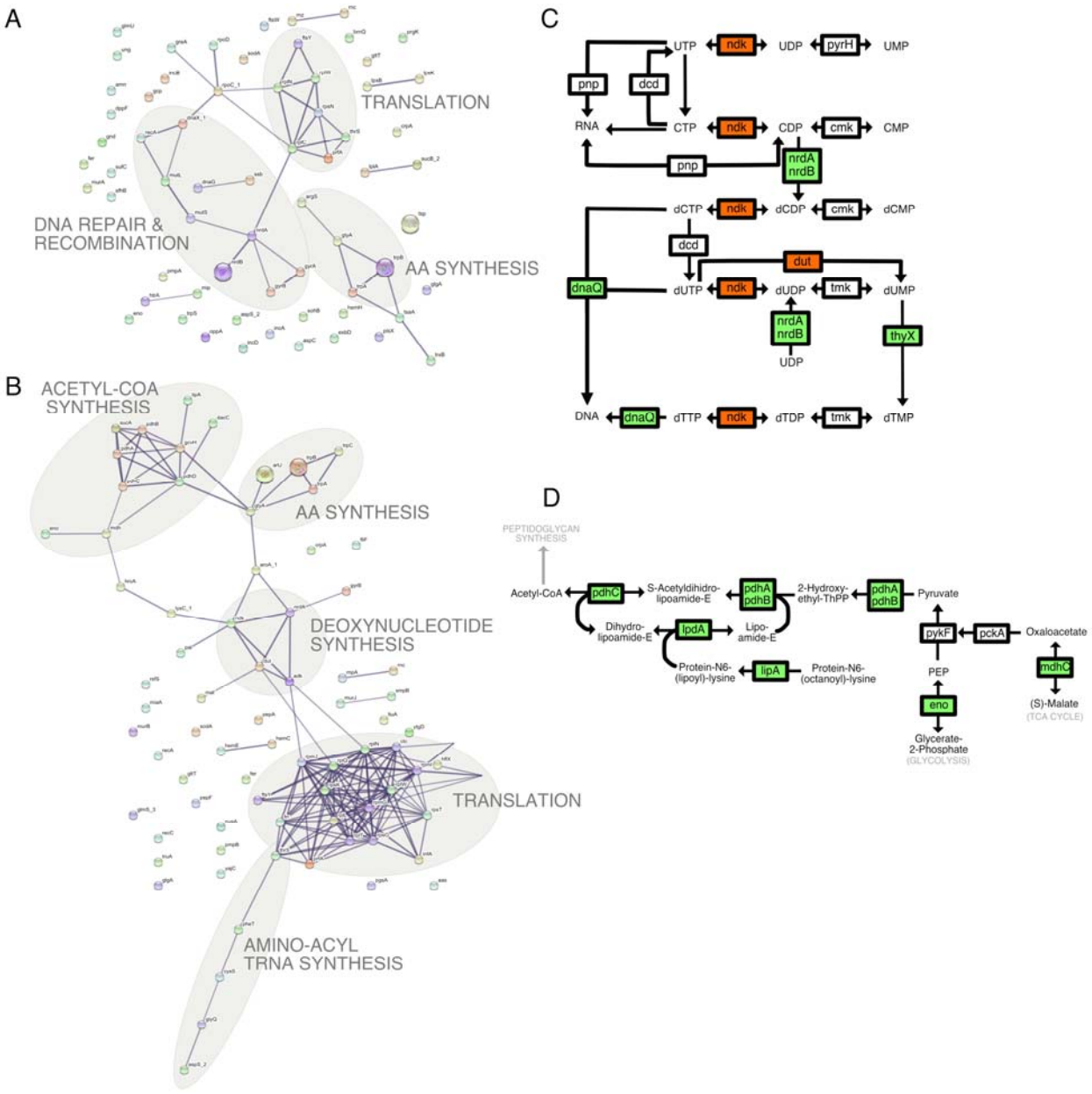

963

964 **Figure 7. Pathway analysis of iron-starvation responses.** Association networks for
965 differentially expressed genes, with a p-value ≤ 0.05, were generated for the A) early-
966 cycle response (6+3h BPDL) and B) mid-cycle response (12+3h BPDL) using STRING-
967 db v.10.5. Line thickness connecting nodes (genes) correlates with confidence of gene
968 association, with a minimum confidence cutoff of 0.7. Mid-cycle clustered genes were
969 mapped to C) nucleotide metabolism and D) acetyl-CoA synthesis pathways using

970 KEGGMapper v.2.8. Up-regulated and down-regulated genes in C) and D) are shown
971 with red and green backgrounds, respectively. Unchanged genes have a white
972 background.

973 SUPPLEMENTARY DATA

974 **Figure S1. Annotated heatmap of BPDL-treated and mock-treated gene**
975 **expression in *C. trachomatis* that corresponds to Figure 2A.**

976 **Figure S2. Annotated heatmap of mid-cycle iron-starvation corresponding to the**
977 **subset in Figure 2B.**

978 **Table S1. Normalized means of mock-treated and BPDL-treated transcription**
979 **during mid-cycle development of *C. trachomatis.*** The mean and $\log_{10}$ mean
980 expression values of genes that showed a significant change in gene expression during
981 normal mid-cycle development, p-value ≤ 0.01 are displayed for the following EdgeR
982 comparisons: 12h vs 18h, 12h vs 15h, 15h vs 18h) These values were used to create
983 the heatmaps in Figure 2A. Genes that had at least one value that was greater than the
984 4.5 threshold have an asterisk, and the values are displayed in bold.

985 **Table S2. Complete expression profile of *C. trachomatis* during normal**
986 **development.** The RNA-sequencing reads and EdgeR analysis of normal development
987 of *C. trachomatis* was exported from CLC Genomics Workbench 9.5.3. Samples were
988 normalized across the entire dataset by quantile scaling. rRNAs, tRNAs, and Features
989 (genes) with less than 10 reads in all samples were eliminated from the dataset prior to
990 normalization and EDGE analysis. Unique Reads are raw values. Samples were
991 merged from multiple RNA-sequencing chips to obtain a minimum of 8X coverage.

992 **Table S3. Complete expression profile of *C. trachomatis* during mid-cycle iron**
993 **starvation.**

994 The RNA-sequencing reads and EdgeR analysis of iron-starved *C. trachomatis* was
995 exported from CLC Genomics Workbench 9.5.3. Samples were normalized across the

entire dataset by quantile scaling. rRNAs, tRNAs, and Features (genes) with less than 10 reads in all samples were eliminated from the dataset prior to normalization and EDGE analysis. Unique Reads are raw values. Samples were merged from multiple RNA-sequencing chips to obtain a minimum of 8X coverage.

Table S4. Complete expression profile of *C. trachomatis* during early-cycle iron starvation.

The RNA-sequencing reads and analysis of iron-starved *C. trachomatis* was exported from CLC Genomics Workbench 9.5.3. Samples were normalized across the entire dataset by quantile scaling. rRNAs, tRNAs, and Features (genes) with less than 10 reads in all samples were eliminated from the dataset prior to normalization and EDGE analysis. Unique Reads are raw values. Samples were merged from multiple RNA-sequencing chips to obtain a minimum of 8X coverage.

Table S5. Primers used in this study.